

International Journal of Innovations in Science & Technology



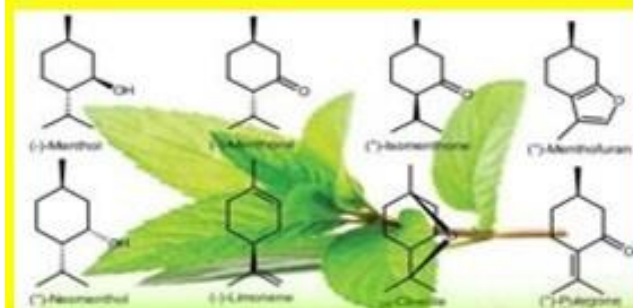
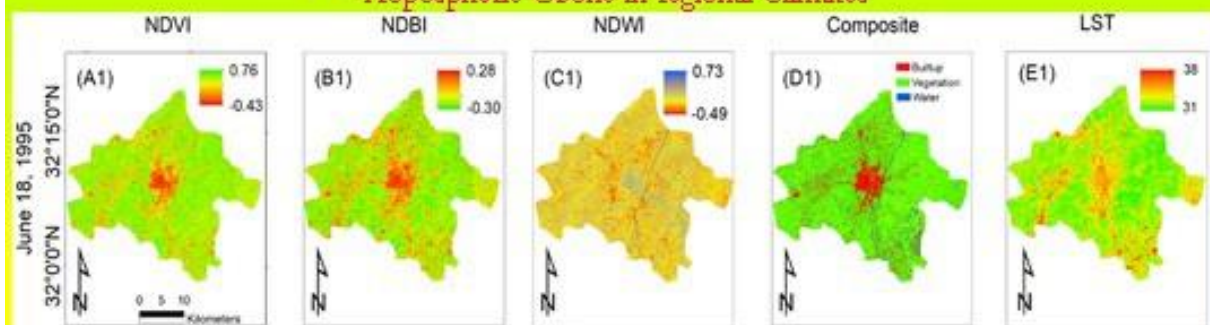
IJIST

Vol 1, Issue 1, Feburay 2019

ISSN 2618-1630

Highlights

Urban Heat Island and our Environment
Preparation of Functional Food to Control Hypertension
Tropospheric Ozone in regional Climates



Journal.50sea.com



Prof Dr. Ali Iqtadar Mirza

Chief Editor

International Journal of Innovations in Science and Technology

Abstracting and Indexing



Instructions for Authors

The editorial board encourages and welcome true researches, laboratory experiments and real time field observations to get published in IJIST. The authors are advised to prepare their manuscript according to the template of IJIST.

Please see the checklist before submitting your manuscript to IJIST.

- The manuscript is prepared according to the template of IJIST.
- Symbols and names are used according to international standards.
- Page no and Line no are adjusted on the manuscript.
- Figure and Table are clearly cited.
- Author names and their affiliation are typed clearly.
- There is no any limit to the length of manuscript.
- Abstract is comprised of 250 words.
- Author's contribution and the statement narrating no of conflict of interest is mentioned in the end.
- Each Figure and Table is numbered and cited in the text.
- Spelling and English grammar is checked.
- It is "Open Access" journal that publish articles on payment of publishing fee by authors or by their institutions.
- All the articles are published under Creative Common License CC-BY therefore, authors mush agree with same license.

Aims and Scopes

The authors are advised to submit their manuscript in accordance with disciplines as below:

- Administrative Science
- Agriculture/Forestry
- Climatology
- Criminology
- Development Study
- Environment
- GIS
- Geography
- Meteorology
- Physics
- Remote Sensing
- Social Science
- Urban Planning
- Economics
- Chemistry
- Bio-Chemistry
- Computer Science

Peer Review Process

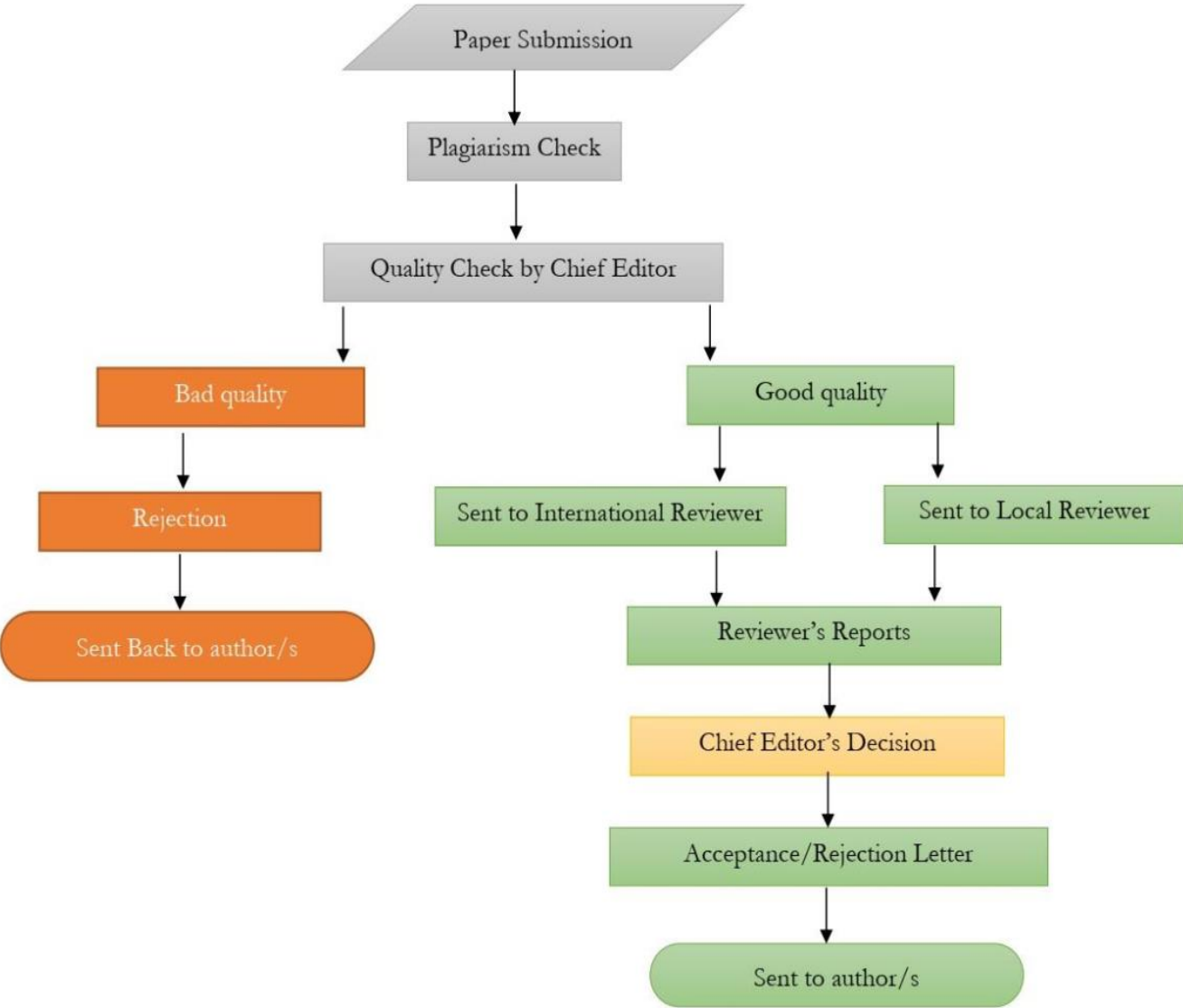


Table of Contents

**International Journal of Innovations in Science & Technology
(IJIST)**

ISSN 2618-1630

V1-I1 | March 2019

Sr No	Items	Page No.
1.	Appraisal of Urban Heat Island over Gujranwala and its Environmental Impact Assessment using Satellite Imagery (1995-2016).	1-14
2.	Preparation of Marketable Functional Food to Control Hypertension using Basil (ocimum basillium) and Peppermint (mentha piperita).	15-32
3.	Additions of Tropospheric Ozone (O ₃) in Regional Climates (A case study: Saudi Arabia)	33-46



Appraisal of Urban Heat Island over Gujranwala and its Environmental Impact Assessment using Satellite Imagery (1995-2016).

Syeda Areeba Gillani^{1*}, Saif-ul-Rehman², Hafiz Haroon Ahmad¹, Abdul Rehman¹, Sarwar Ali¹, Atif Ahmad¹, Usama Junaid¹, and Muhammad Zubair Atiq¹.

1 Remote Sensing group, Department of Space Science, University of the Punjab, Quaid-e-Azam Campus, Lahore, Punjab, Pakistan.

2 Department of Geography, Government College University Lahore.

*Correspondence | Syeda Areeba Gillani E.Mail. syedaareebagillani@gmail

Citation | Gillani.S.A, Rehman.S, Ahmad.H.H, Rehman.A, Ali.S, Ahmad.A, Junaid.U, and Ateeq.Z Appraisal of Urban Heat Island over Gujranwala and its Environmental Impact Assessment using Satellite Imagery (1995-2016). International Journal of Innovations in Science and Technology, Vol 01 Issue 01: pp 1-14, 2019.

DOI | <https://doi.org/10.33411/IJIST/2019010101>

Received | Dec 14, 2018; Revised | Jan 24, 2019 Accepted | Jan 25, 2019; Published | Jan 28, 2019.

Abstract. Rapid urbanization and concretization are the main sources of formation and existence of Urban Heat Island (UHI). Due to high concentration of pollutants in urban environments, the residents are exposed to unexpected health issues. This study aims at delineating the temporal variations in the spatial extent of UHI over Gujranwala using Landsat thermal imagery. It also aims at determining the variations in pollutant concentration in the atmosphere due to vehicle's tailpipe emissions and fossil fuel burning by industrial plants. We used various indices e.g., NDVI, NDBI, NDWI and land surface temperature calculations to investigate spatiotemporal variations in urban growth patterns and their impacts on the UHI. The results show that the UHI enlarged in all direction specially in the north west during the study period which is similar to urban growth trends. There also exist positive correlation between industrial and vehicle's discharge with pollutant's concentration in atmosphere. Remote sensing tools proved elegant in trend mapping and analysis.

Keywords: Urban heat island, Normalized Difference Vegetation Index (NDVI), Normalized Difference Built-up Index (NDBI), Normalized Difference Water Index (NDWI), Land Surface Temperature (LST).

1. Introduction.

The recent migration trends of masses toward developed cities in search of basic needs of life is very common around the world. It is the main reason of extensive urbanization [1] which has transformed the metropolitan areas into heat islands [2] and this phenomenon is termed as Urban Heat Island (UHI) [3]. The speedy urbanization has enhanced the anthropogenic activities that have led to the development of urban microclimates. Microclimates are getting warmer due to many factors including tailpipe emissions by vehicles used for transportation, fossil fuel and coal burning by industrial plants and the cooking concentration at domestic and commercial level [1]. The growth of vehicles adds greenhouse gasses and Chloro Fluoro Carbons (CFCs) in the atmosphere which absorb the outgoing long wave radiations that contribute to increase the city temperature more than periphery. Urban heat islands are of two types: 1) Atmosphere heat island 2) Surface heat island. The atmospheric heat island is further subdivided in two types: 1) Urban canopy layer; and 2) Urban boundary layer.

The surface heat island can be studied in detail due to availability of freely available remotely sensed datasets [3]. These datasets have motivated researchers to investigate the main sources of urban heat reservoirs currently available worldwide [4]. The urban heat can be analyzed by extracting the Land Surface Temperature (LST) through satellite derived data. A wide range of thermal datasets recorded by various sensors including Advanced Spaceborne Thermal Emission and reflection (ASTER), Advanced Very High Radiometer (AVHRR), Moderate Resolution Imaging Spectrometer

(MODIS), Landsat 5 Thematic Mapper (TM), Landsat-7/Enhanced Thematic Mapper (ETM) and Landsat-8 (TIRS 1,2) are useful to extract the pixel-based surface temperature. Various researches have focused on the relationship of Land Use Land Cover (LULC) with LST [5], and found that the changes in LST are dependent upon the spatial arrangement of urban settlements.

The natural vegetation is the main source of carbon sinks which is removed to established new settlements [6, 7]. The negative impacts of new settlements are extensively studied to determine the influence of LULC on urban environment e.g. Ding et al., 2013 [8] investigated the relation of LULC with LST using Landsat images. Similarly, Jusuf et al., 2007 [9] used LST data to explore the consequence of LULC changes on the spatiotemporal pattern of UHI in Singapore. Zang et al. 2013 [10] evaluated the rate of increasing population on UHI patterns in Shanghai. Li et al., 2011 [11] computed LST and Normalized Difference Vegetation Index (NDVI) to understand the impacts of urban sprawl on the landscape of Shanghai. Kuang et al., 2015 [12] examined the difference of LST for different LULC classes and pointed out that urban areas were found warmer than vegetative areas. The thermal properties of land have been altered by modification in LULC of an area that causes the change in energy budget, creating the UHI. Zhang 2008 [13] studied various urban factors including urban area, water body, vegetative area, and the mean NDVI to map the spatial extent of UHI. Singh 2004 [14] monitored the seasonal variations in LST of Dehli using Landsat TM data. NDVI is a common indicator used to discriminate the vegetation existing in an area from other features like built-up area and the water body [15]. Lo et

al., 2003 [16] used NOAA-AVHRR data to compute temporal variations in NDVI and LST to map LULC changes in Iberia. Similar studies were conducted by Kawashina 1994 [17] for Tokyo, the pearl river delta China [18], the Atlanta metropolitan area [15, 19, 20] through Landsat thermal datasets. Many other studies explored the relationship between LST, land surface emissivity and NDVI [21, 22, 23, 24]

The main objectives of this research were to delineate the temporal variations in the spatial extent of urban heat island over Gujranwala and to appraise the impacts of various pollutants involved in heat traps using satellite images from (1995-2016) in ARC GIS interface.

2. Materials and methods.

2.1 Investigation site.

Gujranwala is among the seven most populous areas in Pakistan. It is located in northeast of Punjab province in Pakistan. It is bordered by the districts including Sheikhupura in the south, Hafizabad, and Gujrat in west and Sialkot in the northeast. Gujranwala is known as a third largest industrial center after Karachi and Faisalabad in Pakistan that contributes to 5% in national Gross Domestic Product (GDP)(Gujranwala Wikipedia <https://en.wikipedia.org/wiki/Gujranwala>). It has hot and semi-arid climate where temperature ranges between 36 to 46 °C in summer and drops to 5 °C in winter. The spatial extent of Gujranwala is mapped in Figure 1.

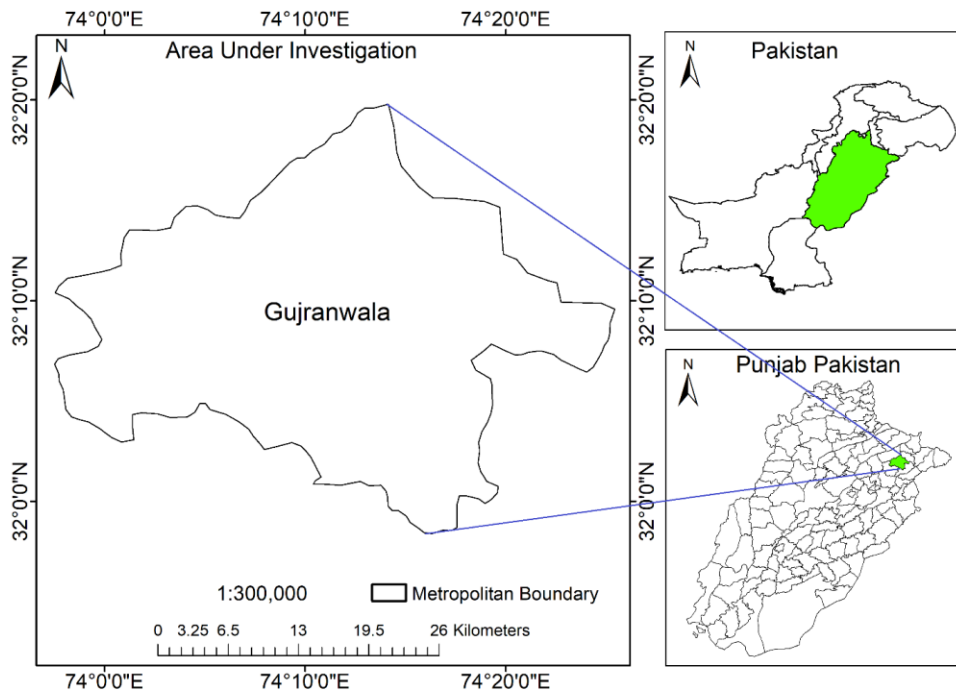


Figure 1. Study site.

2.2 Material and methods.

The spatiotemporal patterns of LST are explored and compared using various indices including NDVI, Normalized

Difference Built-up Index (NDBI) and the Normalized Difference Water Index (NDWI). The contemporary advantage of this research was to use remote sensing data in wider issues relating to the impacts of variations in NDVI and LST on the environment and human health. We used Landsat satellite imagery listed in Table 1, freely available on United State Geological Survey (USGS) website (<https://earthexplorer.usgs.gov>) to estimate the spatiotemporal variations in vegetation, built up and water indices. Thermal datasets are the valuable products of Landsat series that return pixel-based temperature values.

Table 1. Landsat image acquisition dates.

Sr No	Date	Landsat Series
1	June18, 1995	Landsat 5
2	May 06, 2000	Landsat 7
3	June 21, 2005	Landsat 5
4	June 11, 2010	Landsat 5
5	May 26, 2016	Landsat 8

2.3 Pixel-based temperature calculation for Landsat 8 thermal bands.

Landsat 8 started functioning on April 10, 2013, with a wider range of spectral bands within visible, infrared and thermal wavelengths. Band 10 (B10) and Band 11 (B11) are known as thermal bands commonly used to compute pixel-based temperature values. A thermal dataset is comprised of an array of pixels and each pixel preserves a unique number called Digital No (DN). Initially, the DN values are converted to irradiance using Equation 1 as below,

$$\text{Irradiance} = (3.342 \times 10^{-4} \times \text{Thermal band}) + 0.1 \quad (1)$$

The value 3.342×10^{-4} is mentioned in the metadata file (.MTL) saved by a complete Landsat image. Equation 1 is useful to extract pixel-based irradiance in (watt/m²srad). The irradiance-based dataset is further converted to temperature using the Equation 2 as below,

$$T = \left(\frac{K_2}{\ln(\epsilon K_1 / \text{Irradiance} + 1)} \right) - 273 \quad (2)$$

Where K_1 and K_2 are constants and their values are mentioned in the metadata file of each Landsat 8 image as below.

K_1 for B10 = 774.89

K_1 for B11 = 480.89

K_2 for B10 = 1321.08

K_2 for B11 = 1201.44

Where ϵ is emissivity and its value is taken as 0.95 [25]. The complete procedure of extraction of pixel-based temperature values is mentioned on USGS website. (http://landsat.usgs.gov/Landsat8_Using_Product.php).

2.4 Pixel based temperature calculation for Landsat 5,7 thermal bands.

Thematic Mapper (TM) in Landsat 5 and Enhanced Thematic Mapper Plus (ETM+) in Landsat 7 also offer thermal band B6. However, the procedure to analyze pixel-based temperature variations is quite similar for the both thermal bands produced by TM and ETM+ [26]. Initially, the DN values are converted to spectral radiance using the Equation 3 as below,

$$L_\lambda = L_{\min} + (L_{\max} - L_{\min}) \times \text{DN} / 255 \quad (3)$$

Where L_λ is spectral radiance, L_{min} and L_{max} are the variations in radiance. The values assigned to L_{min} and L_{max} are 607.7 and 1260.56 respectively. We used the Equation 4 to extract pixel based temperature values in centigrade

$$T = \left(\frac{K_2}{\ln(K_1 / L_\lambda + 1)} \right) - 273 \tag{4}$$

2.5 Calculation of built up, vegetation and water indices.

NDVI is a vegetation index commonly used to determine the spatial extent and health of vegetation in an area. It is widely used index that considers a spectral band within near infrared wavelength and the other in red wavelength using the Equation 5 below [4, 18, 20].

$$NDVI = \frac{NIR - Red}{NIR + Red} \tag{5}$$

NDVI ranges between -1 to +1 where +1 highlights the vegetation and -1 represents all the feature other than vegetation.

NDBI is commonly used index to map the built-up areas and barren lands. Built-up areas experience a drastic increase in reflectance in the Shortwave Infrared (SWIR) wavelength range (1.55-1.75) μ m and are markedly lower in the Near Infrared (NIR) wavelength i.e., (0.76-0.90) μ m. The differentiation between these two wavelength ranges results in positive values for built-up pixels [27] as follows,

$$NDBI = \frac{SWIR - NIR}{SWIR + NIR} \tag{6}$$

NDWI is the water index that is commonly used to enhance the reflectance of

water bodies within a study site. The formula used to compute NDWI is as follows,

$$NDWI = \frac{Green - NIR}{Green + NIR} \tag{7}$$

Water reflects maximum in green wavelength range (0.52-0.60) μ m and absorbs all the heat radiations within NIR range.

2.6 Regression analysis.

Regression is a statistical indicator used to determine the strength of the relationship between two variables. We used regression to compute the relationship for spatiotemporal variations between concentrations of various pollutants in comparison to their sources.

2.7 GIOVANNI.

GIOVAANI is web-based forum sponsored by National Aeronautics and Space Administration (NASA) that provides spatiotemporal variations in concentration of atmospheric gases globally. We used GIOVANNI to extract the information about atmospheric constituents that play a vital role in increasing the LST by capturing the terrestrial heat.

Results and discussion.

We selected the satellite imagery for the months May and June to compute the vegetation indices e.g., NDVI, NDWI, and NDBI for the study site. During these months the study area receives maximum sunshine hours and peak solar flux which is important to delineate UHI. Also, we can get high contrast for the indices to map the extent of major features including built-up area, water body, and the vegetation. NDVI is an important indicator commonly used to map the spatial extent of vegetation existing in an area. We used Equation (5) to generate

NDVI based datasets for all satellite images mentioned in Table 1 using spectral bands in NIR and red wavelength ranges and mapped the results in Figure (2) A1-A5, where the lush green areas are vegetation and the red regions are non-vegetative features. NDBI is an elegant indicator that highlights the built-up features including buildings, road networks and open areas etc. This index is used to distinguish urban areas in comparison to other features like vegetation or water body. We used Equation (6) to generate NDBI based datasets for all Landsat images mentioned in Table (1) using the spectral bands in SWIR and NIR wavelength ranges and mapped the results in Figure (2) (B1-B5). NDWI is an index which is used to make prominent the water body existing in a dataset. Water is a good absorber of heat in infrared wavelength that reflects nothing toward satellite's sensor, therefore, we get waterbody in blackish tone in a remotely sensed dataset hence water area is difficult to demarcate properly. NDWI is used as a substitute to delineate water features existing in an area. We applied Equation (7) to all the datasets mentioned in Table 1 to delineate the water body and mapped results in Figure 2 (C1-C5).

Temperature effects the human activities and consumption of biomass of an area. Various crop promoting activities to achieve targeted productivity level is operated by temperature. These activities

include 1) the impact assessment of net radiations on plant growth 2) the effects of elevated temperature on biomass generation and 3) the effects of heat stress on the water intake capacity by plants, therefore, it is important to manage the temperature range which is considered optimum for the proper growth of a particular plant.

The heat generation in an area is largely dependent upon various factors including the existing land use, number of vehicles, industrial emissions, and burning of fuels. The temperature of the study site is increasing every year that needs to be monitored to create a balance between the urban area in comparison to its surroundings. We computed pixel-based temperature datasets using thermal bands for all satellite images mentioned in Table 1 and mapped the results in Figure 2 (E1 to E5). We extracted vegetation from all NDVI based datasets, built-up areas from NDBI datasets, water from NDWI based datasets and made composites by taking their integrated impact e.g., the composite made for the year 1995 consisted of the collective impact of three indices using raster calculator utility in Arc GIS 10.1. This method of generation of composites is comparatively accurate as per other methods of feature mapping using classification utility. We used Equations (1,2) for thermal datasets of Landsat 8 and the Equations (3,4) for Landsat 5,7 to compute pixel-based temperature values.

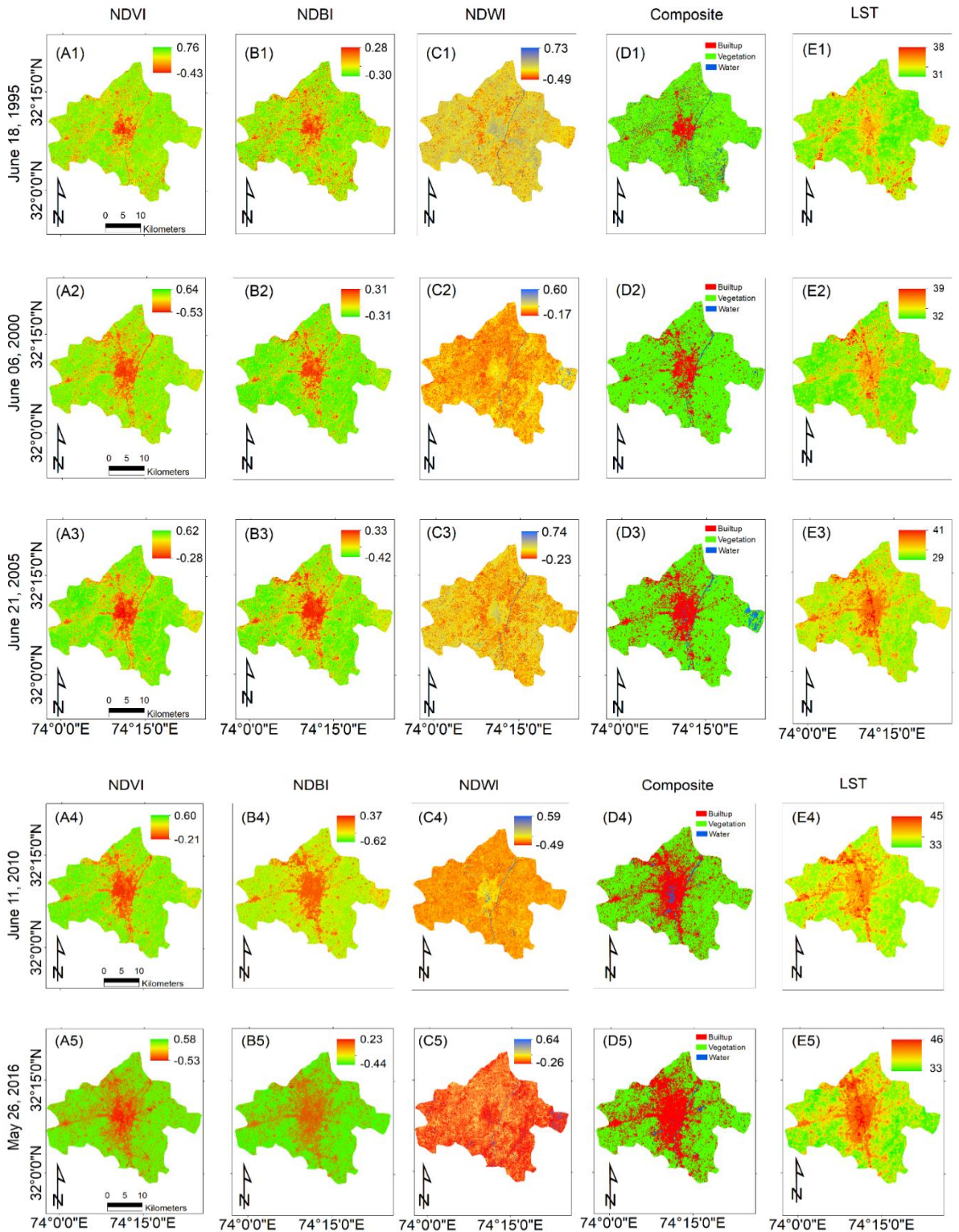


Figure 2. Spatiotemporal variations in NDVI, NDBI, NDWI and LST (°C).

Spatiotemporal variations mapped in Figure 2 determine that the total area under investigation was 861 km². This area was partitioned by three dominating features including built-up area, water body, and the vegetation. The maps (A1 to A5) in Figure 2 are showing a decline to the vegetative area of 725 km² was under vegetation in the year 1995 that degraded to 320 km² in 2016. Whereas the maps (B1 to B5) in Figure 2 describes progressive jumps to built-up area. Built up area was estimated as 93 km² in 1995 that increased up to 318 km² in 2016. Built-up area was observed with a remarkable boost of 78 km² during 2010 to 2016. The maps (C1 to C5) in Figure 2 highlights the water body which seems with no change in area under water flow. The water area was observed as 43 km² in 1995 that remained unchanged in 2016. We observed a slight increase in water area in the map C4 in Figure 2 which was the accumulation of rainfall water that removed after some days by evaporation and seepage by the earth. The composites containing an amalgam of all existing features were mapped (D1 to D5) in Figure 2 which show a degradation to vegetation in comparison to built-up areas. Spatiotemporal variations in land use patterns (D1 to D5) were analyzed that determine the temporal shift of built-up areas toward north-west direction at large scale and a reasonable sprawl in all directions at small scale. Maps (E1 to E5) in Figure 2 determines the spatial variability of lands surface temperature. The comparison of maps (D1 to D5) with (E1 to E5) in Figure 2 shows the same trend for hotspots marked with red color which means that the spatial extent of heat islands is highly dependent on

built-up land use patterns, e.g., the shape of heat island in map E1 was centralized according to the built-up extent mapped in D1 that show similar patterns for heat island as per temporal changes in built-up land use.

2.8 Effects of atmospheric gasses on urban heat islands.

The concentration of various gases e.g., (CO₂, CO, NO₂, and SO₂) plays a vital role in increasing the atmospheric temperature. These gases are capable enough to capture longwave radiations emitted by the surface of earth creating a natural greenhouse effect. The impacts of these gasses cannot be ignored while investigating the UHI phenomenon in an industrial region like Gujranwala therefore, we collected temporal variability of these gasses from GIOVANNI for our study area and analyzed the main sources of production of air pollutants in term of CO₂, CO, NO₂ and SO₂. These pollutants are highly involved in blockage of urban heat and the terrestrial radiations which cause to make the urban areas as heat islands. There are many sources which produce these pollutants but there are two major sources including the fuel burning by the vehicles and the industrial emissions. These emissions cause to increase the concentration of these gases in atmosphere therefore, we collected all the data regarding the temporal increase in a number of industries and the vehicles in Gujranwala from Pakistan Bureau of Statistics annual reports for the years 1995 to 2016 as mentioned in Table 2.

Table 2. Temporal variations in concentrations of CO₂, CO, NO₂ and SO₂ from 1995 to 2016.

Year	CO ppbv	CO ₂ PPM	NO ₂ 1cm ⁻² (x10 ¹⁵)	SO ₂ Kgm ⁻³ (x10 ⁻⁹)	Vehicles	Industries
1995	105	363	4.2	2.6		550
1996	105	365	4.5	2.9		611
1997	104	368	4.7	3.4		684
1998	115	370	4.8	3.1		710
1999	114	371	5	4.6		695
2000	112	373	5.2	4	25730	695
2001	105	375	5.3	4.1	122659	620
2002	110	376	5.3	4.13	132224	641
2003	110	378	5.4	4.15	141789	643
2004	111	379	5.5	4.2	158795	646
2005	109	380	5.6	4.3	183877	646
2006	113	382	5.7	4.4	213771	714
2007	114	383	5.8	4.7	247029	817
2008	114	386	6	4.5	283154	949
2009	115	389	6.3	5	327533	1039
2010	115	392	7	4.6	372733	1056
2011	116	394	8.1	5	422902	1079
2012	117	396	8.6	5.2	474825	1092
2013	118	397	8.8	5.4	534905	1105
2014	121	404	9.1	5.8	640423	1218
2015	124	403	9.3	5.7	689294	1278
2016	130	420	11.5	6.5	796751	2131

We generated a linear regression to determine the strength of relationship of industrial emissions with atmospheric pollutants and mapped the results in Figure 3.

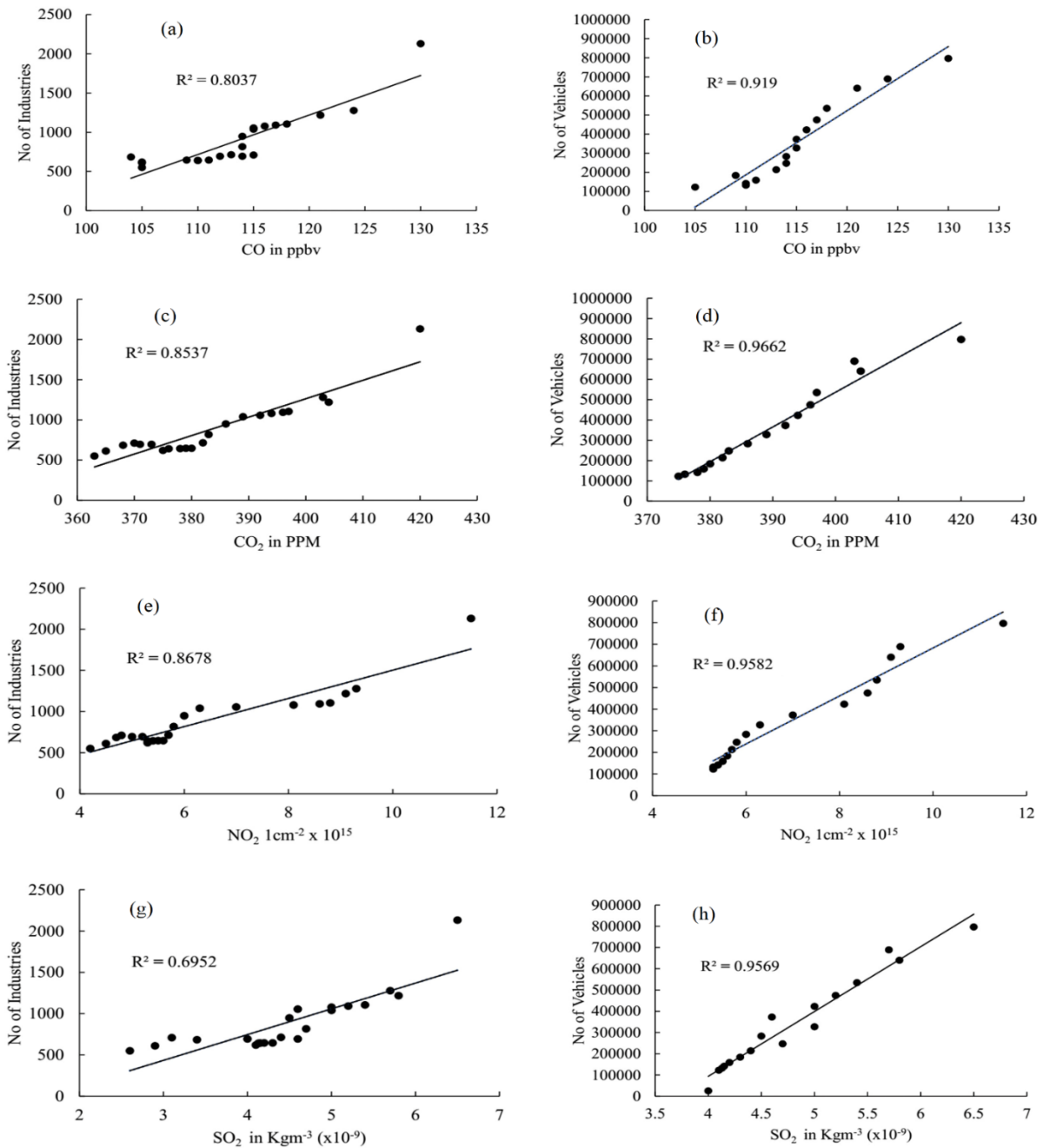


Figure 3. Linear regression model applied to various gasses (CO₂, CO, NO₂ and SO₂) effecting the urban temperatures.

Carbon monoxide (CO) is a colorless, odorless and poisonous pollutant which is formed by fossil fuel combustions emitted by the both vehicles and the

industrial emissions. The number of registered industries in Gujranwala was increased up to 2131 in the year 2016 which was only 550 in 1995. CO concentration in

the atmosphere was largely influenced by industrial emissions as there were 740 industries in 1998 and the CO concentration was 115ppbv as recorded by GEOVAANI that reduced to 110ppbv against 641 industries in 2002. We applied a linear regression model to the increasing concentration of CO in comparison with temporal variation in a number of industries and the vehicles to determine the strength of relationships. We found that CO concentration in the atmosphere was largely influenced by the number of vehicles with $R^2=0.919$ as compared to industries as mentioned in Figure 3 (a,b). CO blocks the heat and creates a natural heat island.

Carbon Dioxide (CO_2) is emitted by tailpipe from trucks, cars, vehicles, and buses. As the number of vehicles increases the concentrations of CO_2 increases in the atmosphere which causes the main source of heat trap in the atmosphere. The burning of fuels by vehicles add a high concentration of CO_2 in the atmosphere as determined by the regression analysis applied in Figure 3 (d) with $R^2 = 0.96$. However, industries added healthy quantity of CO_2 in the atmosphere analyzed using regression analysis of CO_2 with a number of industries that generated $R^2=0.85$ in Figure 3 (c). This large concentration of CO_2 in the atmosphere is capable to block terrestrial heat and to create a heat island.

Nitrogen Dioxide (NO_2) is a pollutant which plays a vital role in making ground-level ozone and particulate matter. It causes the human lungs infection and destroys the immunity system which works in defensive mode against respiratory

infections such as influenza and Pneumonia. Sulphur Dioxide (SO_2) is a very harmful pollutant for the human body that is produced by the burning of diesel and coal. The existence of SO_2 in atmosphere is the clear indication of working of industrial plants. It is highly risky to intake by young ones that cause asthmatic attacks. We generated a correlation between temporal variations of SO_2 concentration in the atmosphere in comparison to the increasing number of vehicles and industries and found a strong relationship for the both as mentioned in Figure 3 (g,h).

3. Conclusion.

Anthropogenic activities played a vital role in enhancing the concentration of atmospheric pollutants in the atmosphere of study site which has created an alarming situation not only for human survival but also for agricultural productivity. The atmosphere of Gujranwala is getting heated and this overheating has influenced the crop phenology and a seasonal shift in local climatic events, therefore, we get rainfall in Gujranwala at the time which is not suitable for crops e.g., in ripening periods. On the other hand, a large number of patients were observed in recent decade in outdoors and emergencies of hospitals who are hit sun stock, dehydration and skin problems. People face a number of health issues which are due to inhale of these pollutants. CO is a precursor of bad ozone and ozone cause skin cancer. Therefore, it is important to take bold steps at the governmental level to control the oxides of Carbon, Sulphur and Nitrogen emissions by controlling of fossil fuels and coal burning

Acknowledgement. We acknowledge earth explorer for provision of valuable data to accomplish this task.

Author's Contribution. All the authors contributed equally.

Conflict of interest. We declare no conflict of interest for publishing this manuscript in IJIST.

Project details. NIL

References

- [1] J. Voogt and T. Oke, "Thermal remote sensing of urban climates.," *Remote Sens. Environ.*, vol. 86, p. 370–384., 2003.
- [2] S. Valsson and A. Bharat, "Urban heat island: Cause for microclimate variations.," *Architecture-Time Space & People*, pp. 21-25, 2009.
- [3] R. Singh and A. Grover, "Remote sensing of urban microclimate with special reference to urban heat island using Landsat thermal data.," *Geogr. Polonica*, vol. 87, pp. 555-568, 2014.
- [4] Q. Weng, L. Dengshang and S. Jacquelyn, "Estimation of land surface temperature—Vegetation abundance relationship for urban heat island studies.," *Remote Sens. Environ.*, Vols. 89,, p. 467–483., 2004.
- [5] R. Amiri, Q. Weng, A. Alimohammadi and S. Alavipanah, "Spatial-temporal dynamics of land surface temperature in relation to fractional vegetation cover and land use/cover in the Tabriz urban area, Iran.," *Remote Sens. Environ*, vol. 113, p. 2606–2617, 2009.
- [6] Q. H.-S. C. J. C. Le-Xiang, "Impacts of land use and cover change on land surface temperature in the Zhujiang Delta," *Pedosphere*, vol. 16, p. 681–689.
- [7] W. C. W. L. D. D. Y. A. Kuang, " comparative analysis of megacity expansions in China and the U.S.: Patterns, rates and driving forces," *Landsc. Urban Plan*, vol. 132, p. 121–135, 2014.
- [8] H. S. W. Ding, "Land-use/land-cover change and its influence on surface temperature: A case study in Beijing city.," *Int. J. Remote Sens*, vol. 34, p. 5503–5517, 2013.
- [9] S. W. N. H. E. A. R. H. Y. Jusuf, "The influence of land use on the urban heat island in Singapore.," *Habitat Int*, vol. 31, p. 232–242, 2007.
- [10] H. Q. Z.-F. Y. X.-Y. C. Y.-B. M. W.-C. Zhang, " Analysis of land use/land cover change, population shift, and their effects on spatiotemporal patterns of urban heat islands in metropolitan Shanghai, China.," *Appl. Geogr.*, vol. 44, p. 121–133., 2013.

- [11] J. S. C. C. L. Z. F. M. X. W. J. Li, "Impacts of landscape structure on surface urban heat islands: A case study of Shanghai, China.," *Remote Sens. Environ.*, vol. 115, p. 3249–3263, 2011.
- [12] W. D. Y. Z. C. C. W. L. A. L. Y. Kuang, R. Zhang and J. Liu, "Quantifying the heat flux regulation of metropolitan land use/land cover components by coupling remote sensing modeling with in situ measurement.," *J. Geophys. Res. Atmos.*, vol. 120, pp. 113–130, 2015.
- [13] J. W. Y. Zhang, "Study of the relationships between the spatial extent of surface urban heat islands and urban characteristic factors based on Landsat ETM+ Data.," *Sensors*, vol. 8, p. 7453–7468, 2008.
- [14] R. G. A. Z. J. Singh, "Inter-seasonal variations of surface temperature in the urbanized environment of Delhi using Landsat thermal data.," *Energies*, vol. 7, pp. 1811–1828, 2014.
- [15] C. Q. D. Lo, "Land-use and land-cover change, urban heat island phenomenon, and health implications: A remote sensing approach.," *Photogramm. Eng. Remote Sens.*, vol. 69, p. 1053–1063. , 2003.
- [16] Y. S. J. M. C. R. A. J.-M. J. S. G. H. V. A. M. F. B. C. J. Julien, "Temporal analysis of normalized difference vegetation index (NDVI) and land surface temperature (LST) parameters to detect changes Iberian land cover between 1981 and 2001.," *Int. J. Remote Sens.*, vol. 32, pp. 2057–2068, 2011.
- [17] S. Kawashima, "Relation between vegetation, surface temperature and surface composition in the Tokyo region during winter.," *Remote Sens. Environ.*, vol. 50, pp. 52–60, 1994.
- [18] X. Z. H. L. P. Y. Z. Chen, "Remote sensing image-based analysis of the relationship between urban heat island and land use/cover changes.," *Remote Sens. Environ.*, vol. 104, p. 133–146., (2006) .
- [19] X. W. P. C. B. Zhang, "Relationship between vegetation greenness and urban heat island effect in Beijing City of China.," *Procedia Environ. Sci.* , vol. 2, p. 1438–1450., 2010.
- [20] Y. Y. C. Q. D. J. P. Zhang, "Study on urban heat island effect based on Normalized Difference Vegetated Index: A case study of Wuhan City.," *Procedia Environ.Sci.*, vol. 8, p. 574–581, 2012.

- [21] J. K. Y. B. B. Mallick, "Estimation of land surface temperature over Delhi using Landsat-7 ETM.," *J. Indian Geophys. Union*, vol. 12, pp. 131-140, 2008.
- [22] R. J. P. Sharma, "Monitoring urban landscape dynamics over Delhi (India) using remote sensing (1998–2011) inputs.," *J. Indian Soc. Remote Sens.*, vol. 41, p. 641–650., 2013.
- [23] Y. B. B. M. J. A. C. K. N. Kant, "Satellite-based analysis of the role of land use/land cover and vegetation density on surface temperature regime of Delhi, India.," *J. Indian Soc. Remote Sens.*, vol. 37, p. 201–214., 2009.
- [24] A. N. P. Acharya, "Population growth and changing land-use pattern in Mumbai metropolitan region of India.," *Caminhos de Geografia*, vol. 11, p. 168–185, 2004.
- [25] S. Raza and S. Mahmood, "Estimation of net rice production through improvedCASA Model by addition of soil suitability constant.," *Sustainability*, vol. 10, no. 6, pp. 1-21, 2018.
- [26] Y. Z. H. K. W. Li, "Monitoring patterns of urban heat islands of the fast-growing Shanghai metropolis, China: Using time-series of Landsat TM/ETM+ data.," *Int. J. Appl. Earth Obs. Geoinf.*, vol. 19, p. 127–138., 2012.
- [27] B. Neela, H. K. Karanam and Victor, "“Study of normalized difference built-up (NDBI) index in automatically mapping urban areas from Landsat TM imagery”," *International J. Remote Sensing*, vol. 8, no. 6, pp. 239-248, 2017.



Copyright © by authors and 50Sea. This work is licensed under Creative Commons Attribution 4.0 International License.



Preparation of Marketable Functional Food to Control Hypertension using Basil (*ocimum basillium*) and Peppermint (*mentha piperita*).

Afshan Saleem¹, Arjumand Iqbal Durrani¹, Fatima Batool Awan², Amina Irfan², Misbah Noreen², M Ali Kamran³ and Duaa Arif².

¹Department of Chemistry, University of Engineering & Technology Lahore.

²Department of Zoology, University of the Punjab Quaid-e-Azam Campus Lahore.

³Department of Physics, University of the Punjab Quaid-e-Azam Campus Lahore.

*Correspondence | Afshan Saleem E.Mail. afshan.jutt66@yahoo.com Department of Chemistry, University of Engineering & Technology Lahore.

Citation | Saleem A, Durrani A.I, Fatima B.A, Irfan A, Noreen M, Kamran A and Duaa A Preparation of Marketable Functional Food to Control Hypertension using Basil (*ocimum basillium*) and Peppermint (*mentha piperita*). International Journal of Innovations in Science and Technology, Vol 01 Issue 01: pp 15-32, 2019.

DOI | <https://doi.org/10.33411/IJIST/2019010102>

Received | Dec 24, 2018; Revised | Jan 22, 2019 Accepted | Jan 25, 2019; Published | Jan 28, 2019.

Abstract.

Functional foods are of great importance which are used to ensure improvements in human health by all aspects. A potential functional food was prepared with five different formulations A, B, C, D and E by using different combination of basil leaf, peppermint leaf and green cardamom to control hypertension. The raw material used for formulation was collected from the local market of Shahdara Lahore in September 2017. Selection of raw materials was totally based on the availability of specified bioactive components which can control hypertension. Formulations A, B, C, D and E were sensory evaluated. The overall acceptability for formulation A was 5/10, B was 6/10, C was 8/10, D was 9/10 and E was 7/10. On the basis of sensory analysis, formulation D was selected. For preliminary analysis, ethanolic and ethyl acetate fraction of basil leaf was prepared. Standard methods of phytochemical analysis were performed to identify flavonoids, alkaloids, polyphenolics and antioxidant activity. Antioxidant activity was measured by using DPPH assay. Quercetin was used as standard. Results were statistically analyzed which showed that IC_{50} ($\mu\text{g/mL}$) value of ethyl acetate fraction (389.00 ± 0.99) was higher than the ethanolic extract (1372.00 ± 6.32) of the basil leaf. On the basis of phytochemical analysis and DPPH assay. We formulated herbal tea that showed promising antioxidant properties. Characterization of food product proved it

as potentially beneficial dietary supplement and hence recommended as potential functional food for hypertension.

Keywords: Hypertension; Functional food; DPPH; Sensory Evaluation and Antioxidant activity.

1. Introduction.

Hypertension or High Blood Pressure (HBP) has become a commonest disease specially in low- and middle-income countries [1]. About 9.4 million deaths occurred due to HBP in the year 2013 [2]. Number of adults suffering from HBP reached up to 13 billion in 2015 around the world. A number of factors are responsible for prevalence of HBP which include excessive intake of sodium products and alcoholic drinks and removal of vegetables and fruits from regular diet. This non-communicable disease can be developed by deficiency of various vitamins such as vitamins C, D, riboflavin and folic acid [3]. Many health organizations emphasized to reduce hypertension through dietary approaches [4]. A healthful life style is the key mechanism to reduce blood pressure. Molarity and cardiovascular diseases are mainly rooted by hypertension. It is proved through many researches that a sodium free diet along with excessive use of fruits may be beneficial against the attacks of hypertension [5, 6, 7]. The main components of healthful diet are fresh fruits, vegetables, grains, nuts, legumes and seafoods. However, the use of red meat and other sodium rich foods are highly restricted in HBP [8, 9, 10].

Functional foods are of great importance which are used to ensure improvement in human health by all aspects [11]. Functional foods are also known as food ingredients which can assist extraordinary in maintaining human health. These are the substances which take a part in growth and development of human bone structure [12]. According to American Dietetic February 2019 | Vol 1 | Issue 1

Association (ADA), the functional foods are enriched foods designed to consume regularly for desired health issues. In 2012, the functional foods were defined in an international conference at Santa Barbara that these are natural or processed foods that contain known and unknown biologically active components in a defined amount which provides a clinically proven and documented health benefits for prevention, management and treatment of chronic diseases [13]. A big variety of functional foods is shown in the Figure 1 as below,



Figure 1. A brief description of functional foods. Modified after Cheryl Tay 2017, <https://www.nutraingredients-asia.com/Article/2017/09/07/Vitafoods-Asia-2017>.

Various foods can be used regularly to maintain the health properly which includes, ginger, garlic, celery and green tea. Garlic is considered as nice addition in regular diet to increase immunity and physical strength to reduce fatigue. Garlic is used in treatment and prevention of various infectious diseases. Cholesterol, blood pressure and cardiovascular health can be maintained by regular use of garlic [14]. Ginger is commonly known as Zingiber Officinale (ZO) that contains anions and

cations with a penalty of magnesium, calcium and phosphorus that functions to improve bone strength and nerve transmission. Ginger is considered best in various health issues like depression, nausea, confusion, weakness, convulsions and gastrointestinal disorder [15]. Moreover, ginger is the main source which regulates heartbeats at regular order [16]. These all foods are considered good to be in taken by patients of hypertension.

Generally, hypertension has no symptoms until serious complications develop that's why it is called "silent killer". There are 2 types of hypertension 1) when the condition has no known cause, it is called Primary Hypertension and this type of hypertension can be controlled but cannot be diagnosed [17, 18]. The diseases which are attributable to hypertension are shown in following Figure 2.

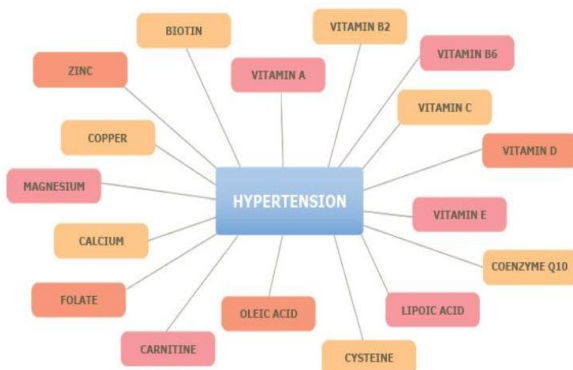


Figure 2. Various factors attributable to hypertension.

The hypertension due to some other indirect diseases/sources is known as Secondary hypertension. Nearly 10-12% of patients are the victim of secondary hypertension, where drug or comorbid are responsible for elevating blood pressure [19]. Hypertension has a variety of causes but in most of these cases, the most common is the deterioration, resulting from serious kidney disease or renovascular disease. Symptoms can differ between individuals depending upon the medical history etc. [20]

The hypertension due to increased peripheral resistance in arterial blood pressure is dangerous for health. It is further divided into 2 types: **a)** Beginning hypertension **b)** Malignant hypertension. The elevation in systolic blood pressure and diastolic pressure is about 200 mmHg and 100 mm Hg respectively. Systolic blood pressure is of 250 mmHg and the diastolic blood pressure is of 150 mmHg. It causes serious problems like retinal and renal diseases. Hypertension is a silent killer so death can cause immediately. [21, 22, 23]. Blood pressure is dependent upon the nature of blood vessels and the distance travelled. Vessels, closer to heart, experience more blood pressure. If the walls of arteries are thicker and less flexible while the vein's walls are thinner and more flexible, this situation leads to low blood pressure [21, 22, 23]. Common determinants of hyper tension are follows, 1) weight is directly related to BP, higher the weight, higher will be the BP, 2) In both male and female, BP generally rises with the age 3). Addiction of Alcohol consumption causes in increase in 4) Burning of tobacco produces nicotine and carbon monoxide that causes hypertension and 5) the survey has been proved that hypertension may be caused by genetic problems. Normal and pulmonary hearts are shown in the Figure 3.

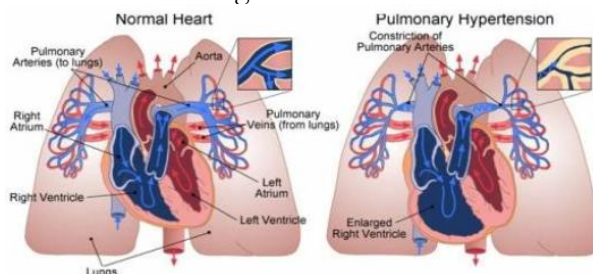


Figure 3. Normal and pulmonary hearts.

The “King of herbs” commonly known as Basil (*Ocimum basilicum* L.) is used in this research for curing hypertension shown in Figure 4. Linalool, eucalyptol, eugenol and chavicol are the essential oils of *Ocimum basilicum*, commonly known as basil. These oils are used as antioxidants. Eugenol is a type of phenolic component which have a large

number of plant sources. Synthesized Eugenol has same properties as that of natural contains. Extracts of numerous medicinal herbs contain significant amount of eugenol that fascinated the attention of several researcher as it can be used as an alternative of medicine to prevent many disorders. World Health Organization (WHO) announced Eugenol as GRAS (Generally Recognized as Safe). Peppermint is used as food additive to enhance the taste as well as antioxidant activity of herbal tea. Cardamom is used for aroma [24, 25, 26].



Figure 4. Basal leaves.

In many cultures and cuisines, basil is an important herb also known as Tulsi which is a spiritual herb in the Hindu religion and considered as holy. British used tulsi as a

replacement of Bible. Bible is holy book of Hindus which is used in a court of law to take an oath [27].

Mentha piperita (Lamiaceae family) which is a common herb that is grown in Europe and North America shown in Figure 5.



Figure 5: Peppermint Leaves

Scientific name of Peppermint is *Mentha piperita*. Peppermint/Black mint is the common names of Peppermint which belongs to Lamiaceae family [28]. Peppermint contains different bioactive compounds like Menthol, Menthone, Isomenthone, Menthofuran, Neomenthol, Limonene, Cineole, and Pulegone etc. as shown in the figure 6.

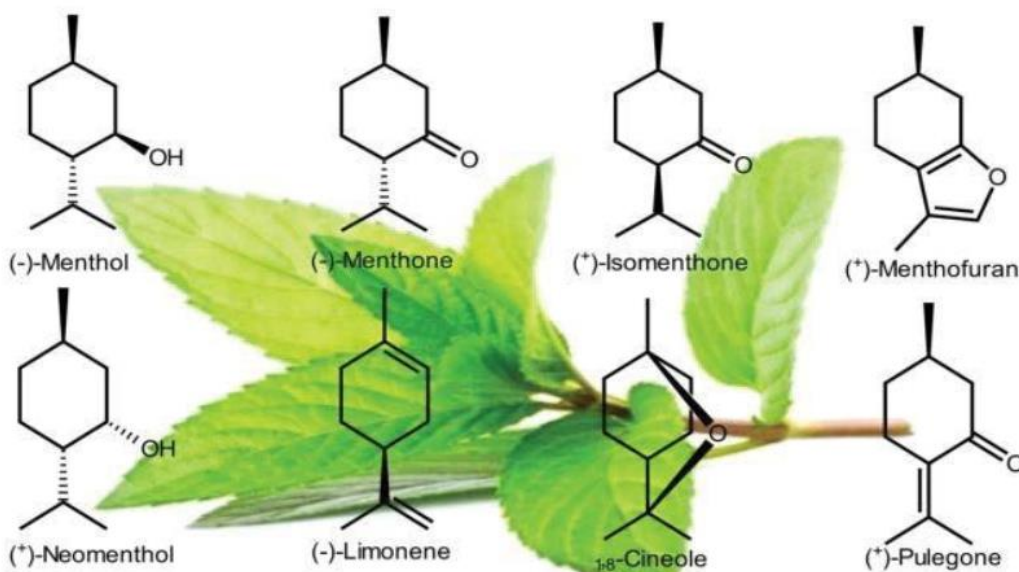


Figure 6: Bioactive compounds of Peppermint
February 2019 | Vol 1 | Issue 1

Peppermint has a lot of health benefits as shown in following Figure 7. It is used as antioxidant,

antiviral, antimicrobial, antispasmodic, antinociceptive, antitumorogenic, anticarcinogenic and allergic. [29]

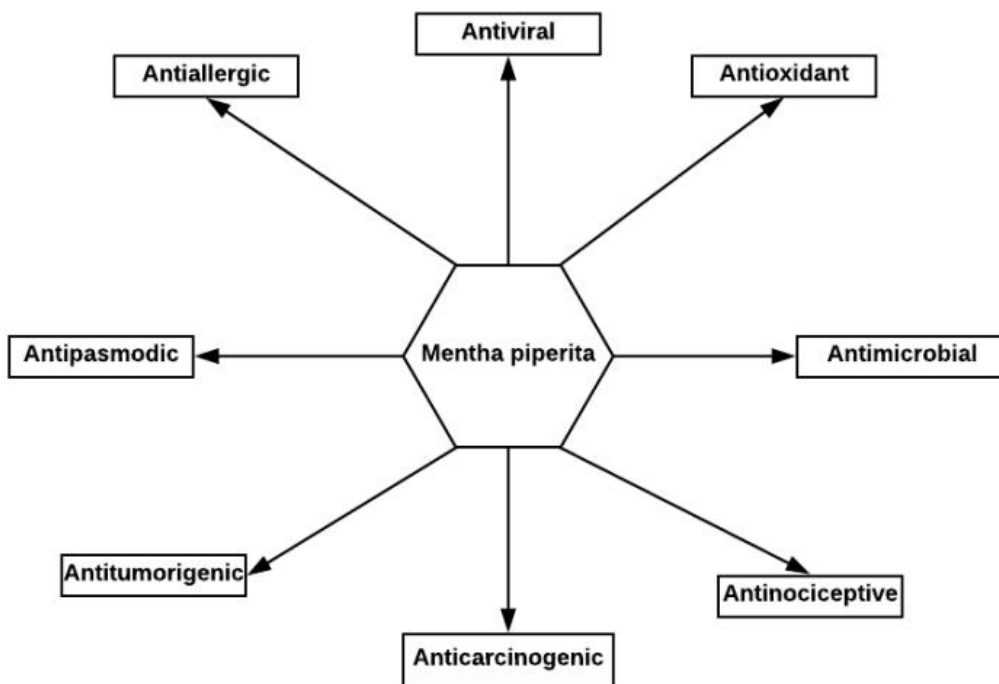


Figure 7: Properties of Peppermint

The main objectives of this research were to prepare a potential functional food to control hypertension.

2. Material and methods.

Sensory evaluation is used in this research which is a specific discipline designed to touch, sight, taste, smell and hear the responses of various food products to analyze similarities and dissimilarities. This technique is defined to determine the gauge of acceptability of a product by all aspects [21]. After sensory evaluation herbal tea was characterized. For Preliminary extraction, ethanolic and ethyl acetate fraction was prepared to identify flavonoids, Polyphenolics, Alkaloids and antioxidant activity. For alkaloids identification, Dragendorff's test, Hager's test, Wagner's test and Mayer's tests were used. FeCl_3 was used for the identification of Polyphenolics and DPPH (2, 2-Diphenyl-1-Picryl-

hydrazyl) was used to check antioxidant activity [30].

2.1 DPPH Compound.

Diphenyl-1-Picryl-hydrazyl is abbreviated as DPPH which is comprised of a stable free radical molecule that are crystalline in nature. These free radicals are atom, ions or molecules which form a dark matter. Free radicals cause oxidation of reduced molecules in cellular structures that includes ischemia, arthritis, atherosclerosis, cancer, gastritis and injury of central nervous system. These radicals can be effectively eliminated with the help of synthetic and natural anti oxidents by their decomposition [31, 32]. DPPH structure is drawn in Figure 8,

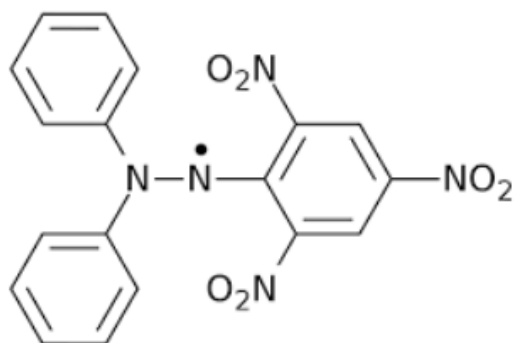


Figure 8. DPPH structure.

UV/VIS Spectrometer.

The ultraviolet and visible portion of electromagnetic spectrum are used in excitation of electrons from ground state to higher energy level. It consists of a light source, monochromator, sample compartment and the detector. The basic structure of UV/VIS spectrometer is drawn in the Figure 9.

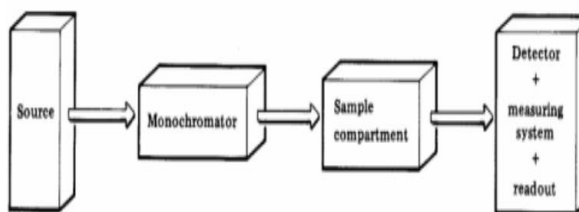


Figure 9. Basic structure of UV/VIS spectrometer.

UV/VIS has large scale use in various analysis e.g., qualitative analysis, dissociation of acids and bases, quantities analysis, pharmaceutical analysis, chemical kinetics and weight determination at microlevels.

Chemicals used in this research.

All the chemicals used in this research work were of analytical grade.

Petroleum Ether: M. mass 82.2 g/mol, colorless, volatile, insoluble in water, soluble in organic solvents, specific gravity 0.64, CAS No. 8032-32-4, Trace SELECT Ultra grade by Sigma-Aldrich.

70% Ethanol (C₂H₅OH): M. mass 46.08 g/mol, colorless, volatile, specific gravity 0.8854, CAS No. 64-17-5, Trace SELECT Ultra grade by Sigma- Aldrich

February 2019 | Vol 1 | Issue 1

Ethyl Acetate (CH₃COOC₂H₅): M. mass 88 g/mol, specific gravity 0.895, colorless, soluble in alcohol and acetone, CAS No. 141-78-6, Trace select Ultra grade by Sigma-Aldrich

Ammonia gas (NH₃): colorless, nonflammable and liquefied gas with strong smell, M. mass 17.03 g/mol, specific gravity 0.597, CAS No. 7664-41-7, Trace SELECT Ultra grade by Sigma- Aldrich

Ferric Chloride Reagent (FeCl₃): Liquid, M. mass 162.195 g/mol, CAS No.7705-08-0, Appearance and odor vary depending upon the specific soluble iron salt, Trace SELECT Ultra grade by Sigma- Aldrich

DPPH (C₁₈H₁₂N₅O₆): Formula name 2,2-Diphenyl-1-Picryl-hydrazyl, crystalline solid, CAS No. 1898-66-4, M. mass 394.3 g/mol, Trace SELECT Ultra grade by Sigma- Aldrich

Mayer's Reagent K₂[HgI₄]: Formula name Mercuric-potassium iodide, Liquid, CAS No. 7783-33-7, M. mass 786.406 g/mol, odorless yellow crystals, Trace SELECT Ultra grade by Sigma- Aldrich.

Quercetin (C₁₅H₁₀O₇): M. mass 302.2 g/mol, CAS No. 117-39-5, crystalline solid, yellow powder, soluble in organic solvents, Trace SELECT Ultra grade by Sigma-Aldrich.

Glassware.

Glassware used in this research is as follows
 1) Beaker: (50 mL, 200mL) 2) Conical flask: (100 mL)40 3) Pipette: (25 mL) 4) Büchner funnel: Porcelain Buchner Funnel, 50 mL
 5)Filter paper: Whatman No. 1, Diameter: 9cm, Pore Size: 11µm and 6)Pestle and mortar

Equipment

Oven: WFO-451SD, max. Temp. reaching time: 60 min, Temp. control range: RT + 10 ~ 270°C, Heater: 1.2 KW, shelf: 2 pcs

Electronic Weighing Balance: TC6K-H, Resolution 0.1g
Magnetic Stirrer: Capacity 2 to 5 liters, temp. up to 200°C

UV-VIS-Spectrometer: Shimadzu 1800 UV/VIS spectrometer, Wavelength range 190-1100 nm, Wavelength repeatability \pm 0.1 nm, photometric system double beam.

Selection of Raw materials.

Raw materials for herbal tea were selected on the basis of availability of specified bioactive components which can control hypertension.

Collection of raw materials

Basil (*Ocimum basilium*) leaves were collected from local market at Abbas nursery, Model town, Lahore in September 2017. Peppermint (*Mentha piperita*) leaves were collected from local market Shahdara Lahore in September 2017. Green cardamom (*Elettaria cardamomum*) was collected from local market Shahdara Lahore in September 2017.

Preparation of raw material

About, 1kg Basil and 0.5kg peppermint leaves were washed in distilled water separately. To avoid thermal decomposition

of antioxidant oils, basil and peppermint leaves were dried in laboratory oven (WFO-451SD, max. temp. reaching time: 60 mint: 2 pcs) at 110°C for 50 min, and at 100°C for 55 min. respectively. Crumbled them separately and stored in a plastic container. Ground green cardamom was grinded in Mortar Grinder RM 200

Formulation of herbal tea.

We used 0.3 g crumbled Basil leaves, 0.1 g crumbled Peppermint leaves and 0.05 g powder of green cardamom and heated. A seal empty tea bag was taken and filled with the mixture. Then we dipped this tea bag in 200 mL hot nestle water to make infusion.

A brief methodology.

In this research, Basil (*Ocimum basillium*) was selected to formulate herbal tea. Peppermint (*Mentha piperita*) and green cardamom (*Elettaria cardamomum*) was used as food additive to enhance its antioxidant effect as well as its taste and aroma. Formulated tea was characterized through sensory evaluation to specify the ratio of ingredients. By using standard methods of phytochemical analysis, antioxidant component of herbal tea was identified. Antioxidant activity was evaluated by using free radical scavenging method. The compound 2, 2-diphenyl-1-picrilhidrazil (DPPH) was used as free radical model.

Flow of methodology,

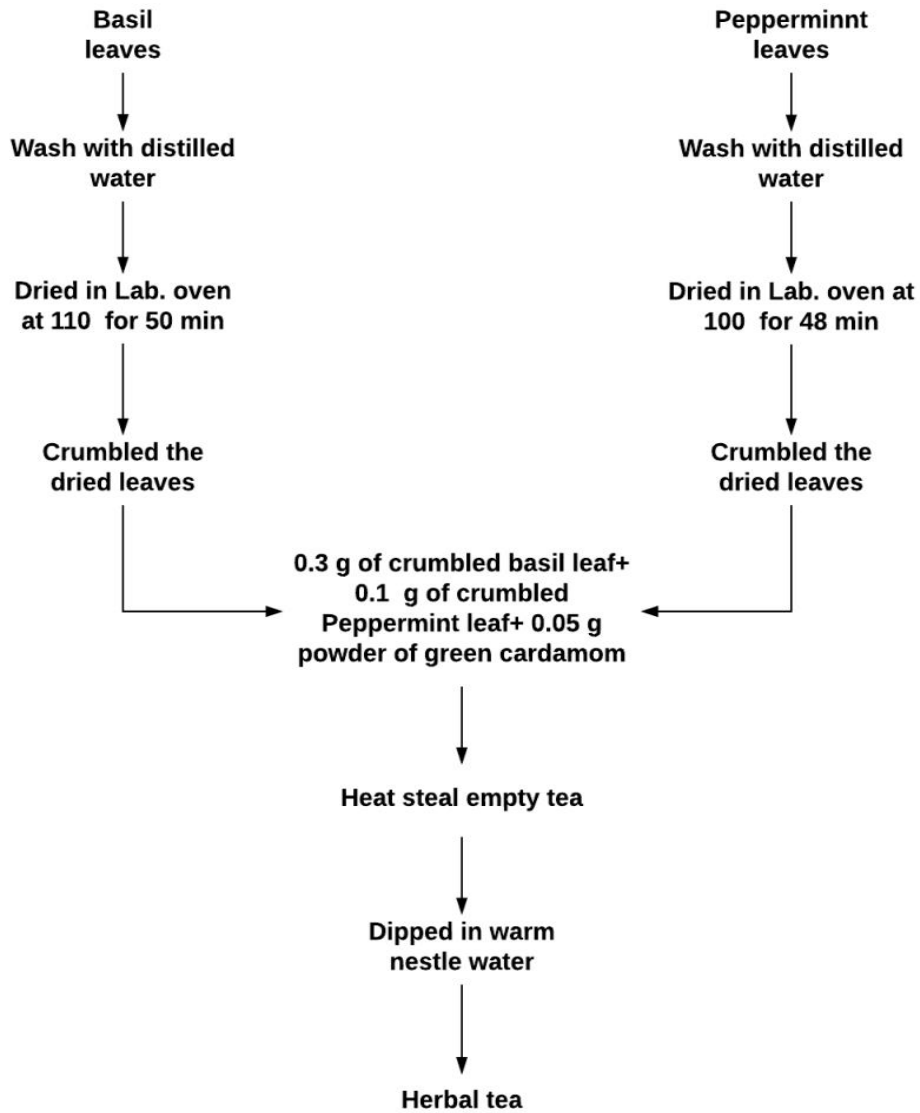


Figure 10. Flow of methodology in preparation of Herbal Tea.

Five different samples A, B, C, D and E of designed functional food product were served to the penal of 5 Judges. The amount of basil and peppermint is listed in Table 1

Sample	Basil	Peppermint	Green cardamom
A	0.1 g	0.1 g	0.05 g
B	0.2 g	0.1 g	0.05 g
C	0.2 g	0.2 g	0.05 g
D	0.3 g	0.1 g	0.05 g
E	0.3 g	0.2 g	0.05 g

Table 1: Five samples of varying amounts of Basil and Peppermint.

Judges were asked to taste the food product and give their remarks as a score out of 10 scale about Aroma, Color, Texture, Taste

and its overall acceptability. On the basis of sensory analysis, a sample was selected and phytochemical analysis were performed by using standard methods to identify alkaloids, flavonoids, Polyphenolics and antioxidant activity.

Preliminary extraction

About 10 g powdered Basil leaf and 40mL petroleum ether was mixed using magnetic stirrer and left the mixture for 1 day in ambient air. After 24 hours the sample was filtered by using Whatman No. 1 filter paper.

Ethanolic extraction

The residue was macerated with 70% ethanol (1:4) then stirrer for 30 minutes using magnetic stirrer and left for 1 day in ambient air. After 24 hours the sample was filtered by using filter paper. The residue was remunerated 2 times. Ethanol was removed from the filtrate using rotatory evaporator at 600C until it became viscous.

Ethyl acetate fraction

About 5 g of viscous extract and warm distilled water was inserted into mortar. Stirred it thoroughly then transferred it into another funnel. Now, we added ethyl acetate to extract suspension in same ratio and shaken it to form 2 layers. The upper layer separated which is soluble ethyl acetate fraction and filtered over Whatman filter paper. Insoluble lower layer was fractionated 2 times with ethyl acetate. We collected the entire soluble ethyl acetate fraction and evaporated it by a rotator evaporator at 600C. After that evaporation continued on water bath until it became viscous.

Identification of flavonoids

One drop of Ethyl acetate fraction and 1 drop of Ethanolic extract was dropped on filter paper separately and let them to dry.

Filter paper with dried droplets steamed using ammonia gas. Which showed dimly yellow to intense yellow to examine the concentration of Flavonoids.

Identification of alkaloids

About 1 mL of Ethanolic extract and same quantity of ethyl acetate was taken for Mayer's reagent. Formation of white precipitate showed that sample contained Alkaloids.

Identification of polyphenolics

About 3 drops of FeCl₃ were added into 1 mL of Ethanolic extract and 1 mL of ethyl acetate fraction. Appearance of Dark black color showed that sample contains Polyphenolics.

DPPH assay

Free radical scavenging method was used for antioxidant activity test. The compound used to perform the activity test was 2, 2-diphenyl-1-picrilhidrazil.

Solution preparation

Stock solutions of each Quercetin (0.2 mg/mL), Ethanolic extract (2 mg/mL) and Ethyl acetate fraction (1 mg/mL) was prepared. From this stock solution further dilutions (50%, 25% and 12.5%) were made. For 0.15 mM DPPH, dissolved 15 mL of 1 mM DPPH in ethanol up to 100ml.

Procedure.

To Perform DPPH test, sample was prepared by mixing 1.0 mL of each dilution in 1.0 mL of DPPH solution. The mixture was shaken well to homogenize and left in darkness for 90 min. Absorbance was measured at 517 nm by using UV-visible spectrometer. Each test is suggested to perform five times. [33]

Results and Discussions.

Sensory evaluation

A panel of 5 Judges tasted 5 different samples of designed functional food and presented their remarks as a score on 10 points scale

Table 2

Table 2: Results of sensory analysis

Sample	Texture	Aroma	Taste	Color	Overall acceptability
A	4	6	3	6	5
B	5	7	5	7	6
C	7	8	7	8	8
D	9	8	8	9	9
E	6	7	5	7	7

It was clear from sensory evaluation that sample C and sample D got maximum points. But sample D got highest points in aroma, texture, color, taste and overall acceptability. Therefore, sample D was selected for phytochemical analysis. Results are shown in Figure 11.

Extraction and fractionation

About 70% ethanol was used to extract the active basil compounds by maceration method. The use of the ethanol is advantageous because it has ability to extract flavonoid compound. In maceration method,

about aroma, color, texture, taste and its overall acceptability. A score above 6 was considered acceptable. Results of sensory analysis are shown in

we diffused the compounds to a low concentration.

Flavonoids identification

Conversion of dimly yellow color into intense yellow color was due to Flavonoids identification by Ethanolic extract and Ethyl acetate fraction. This color conversion indicated the presence of flavonoids. Yellow color occurred due to the formation of quinoid that describes the reactions of ammonia with flavonoids. Quinoid contains a larger conjugated double bond. Results of Flavonoids identification are shown in Figure 12.

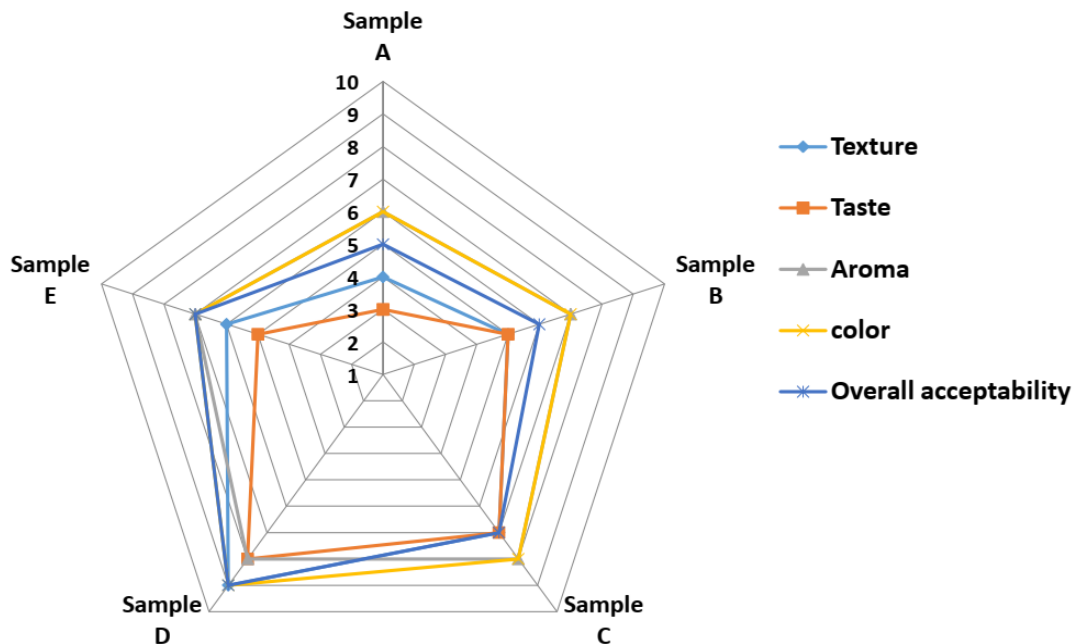






Figure 11. Sensory analysis of five samples.

Alkaloids identification

Formation of white precipitate with Mayer's reagent of Ethanolic extract and Ethyl acetate fraction assisted to identify Alkaloid. Formation of precipitate indicated the presences of alkaloids. In Alkaloids there is a Nitrogen atom present with free electron pair. When Alkaloids react with dipotassium tetraiodomercurat (Mayer's reagent), free electron pair of Nitrogen atom reacts with potassium metal ion through a coordinate covalent bond and potassium-alkaloid is characterized by white precipitate. Results of Alkaloid identification are shown in following Figure 14 and reactions of alkaloids with Mayer's reagent are shown in Figure 15

Polyphenolics identification

When $FeCl_3$ was added in Ethanolic extract and Ethyl acetate fraction, Green-brown color of Ethyl acetate fraction and Brown-black color of Ethanolic extract was changed into Black-brown color which showed that the sample have Polyphenolics compounds. When hydroxyl groups, present in Polyphenolics compounds, react with $FeCl_3$ then Flavonoid- Fe^{+3} complexes were formed. Identification of polyphenolics is shown in Figure 16 and the reaction of Polyphenolics with $FeCl_3$ is shown in Figure 17.

Samples	Samples Solution	Samples with ammonia
Ethyl acetate fraction	 Dimly yellow	 Intense yellow
Ethanollic Extract	 Dimly yellow	 Intense yellow

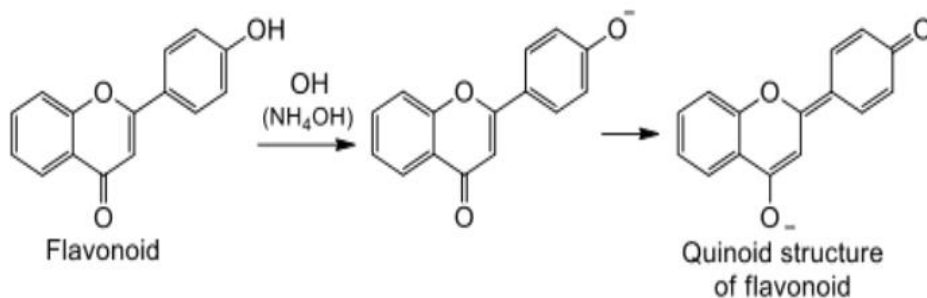


Figure 12. Identification of Flavonoids using ammonia.

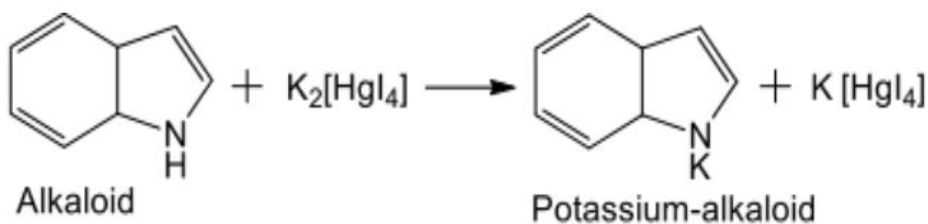
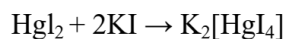
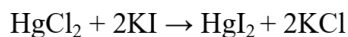


Figure 14. Reaction of Alkaloid with Mayer's reagent.
Mayer's reagent can be prepared from mercury and potassium iodide.



Dipotassium tetraiodomercurat(II)





Samples	Samples solution	Samples with Mayer's reagent
Ethyl acetate	 Green-brown	 White precipitate
Ethanolic Extract	 Brown-Black	 White precipitate

Figure 15. Identification of Alkaloids with Mayer's reagent

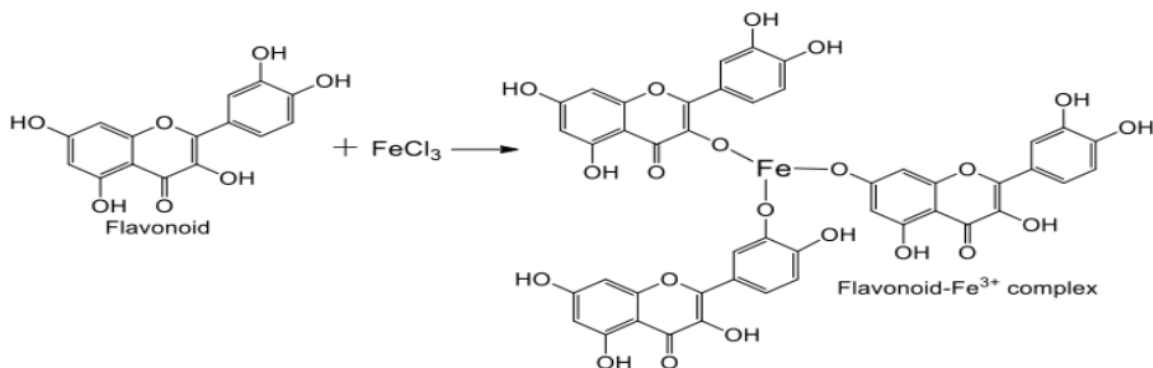


Figure 16. Reactions of polyphenolics with FeCl₃.





Samples	Samples solution	Samples with FeCl ₃
Ethyl acetate fraction	 Green-brown	 Black-brown
Ethanollic Extract	 Brown-black	 Black-brown

Figure 17. Identification of polyphenolics with FeCl₃.

DPPH assay.

DPPH is very popular stable, natural and free radical used for anti-oxidant assay. It has free electrons, delocalized over entire molecule and responsible for its deep violet color in ethanolic extract and ethyl acetate fraction. Anti-oxidant effect of test sample is proportional to the disappearance of DPPH color from reaction mixture. Color of the test sample changes from dark violet to light yellow. Anti-oxidant effect of basil leaves extract in ethanol and ethyl acetate fraction was measured by making their dilutions (3mg/mL, 2mg/mL, 1.75mg/mL, 1.5mg/mL and 1mg/mL). DPPH shows maximum absorption peak at 517 nm indicating its deep color. Color of the solution change from violet to light yellow in the presence of DPPH as shown in Figure 18.

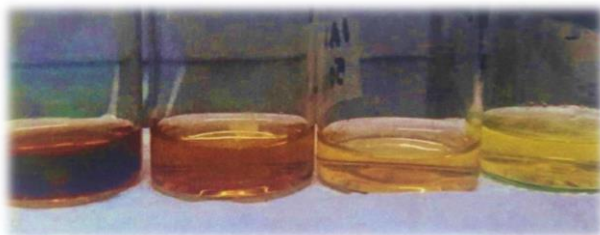


Figure 18. DPPH assay, percentage scavenging increased by increasing amount of Basil leaves.

Anti-oxidant potential increases by increasing the concentration of Basil leaves into solution. The results of antioxidant activity showed that potential activity of ethyl acetate fraction was higher than ethanolic extract of the basil leaf but less than Quercetin. Results are shown in Figure 19.

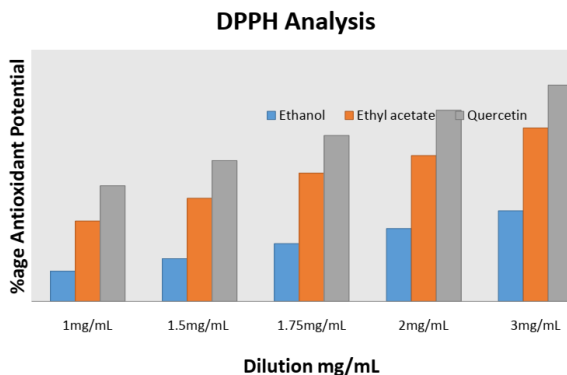


Figure 19. Antioxidant activity of Basil leaves in Ethanol, Ethyl acetate and Quercetin

Statistical analysis

Percentage scavenging radical was measured by following formula:

$$\% \text{age of scavenging radical} = \left(\frac{\text{Absorbance of control} - \text{Absorbance of sample}}{\text{absorbance of control}} \right) \times 100$$

IC₅₀ is defined as an amount of sample required to decline in DPPH absorbance up to 50%. The values of Quercetin, Ethanolic extract and ethyl acetate were computed using SPSS which were computed as 95% confident. The antioxidant activity is shown in Table 3

Table 3. CV percentage of various samples.

Sample	IC ₅₀ (µg/mL)	CV (%)
Ethanolic extract	1372.00±6.32	0.46
Ethyl acetate fraction	389.00±0.99	0.25
Quercetin	2.10±0.01	0.48

The results of antioxidant activity showed that potential antioxidant activity of ethyl acetate fraction was higher than ethanolic extract of the basil leaf, but less than Quercetin. Finally, a potential food is shown in the Figure 20.



Figure 20. Prepared Food product.

Conclusion

A potential functional food was successfully prepared to control hypertension. Sensory evaluation showed that herbal tea tastes good and met the level of hedonic demand. Phytochemical analysis showed the availability of flavonoids, alkaloids and Polyphenolics. Antioxidant potential of basil leaf was measured through DPPH assay. It was confirmed that basil is a good source of antioxidant activity. On the basis of these characterizations it was confirmed that basil leaf can be used to control hypertension.

Recommendations.

This food product can be easily prepared on commercial scale. Composition can be varied according to the consumer demands and as per condition of blood pressure patient. Herbal tea could be prepared with the sweet taste by using specified amount of honey. Sugar patients may use this herbal tea without addition of honey. Cardamom can also be replaced with Lemon, Cinnamon, Cloves and honey as food additive. Shelf life of herbal tea could be enhanced by using preservatives. Use of this herbal tea twice in a day can significantly control hypertension.

Acknowledgement. We acknowledge this work to Chemistry department, University of the Punjab Lahore.

Author's Contribution. All the authors contributed equally.

Conflict of interest. Authors declare no conflict of interest for publishing this manuscript in IJIST.

1.0 Project details. NIL

References

- [1] W. H. Organization., "Información General Sobre la Hipertensión en el Mundo–OMS.," http://apps.who.int/iris/bitstream/10665/87679/1/WHO_DCO_WHD_2013.2_spa.pdf, 2013.
- [2] W. H. Organization, "Global Health Risks Global Health Risks. Mortality and Burden of Disease Attributable to Selected Major Risks," http://www.who.int/healthinfo/global_burden_disease/GlobalHealthRisks_report_full.pdf
- [3] D. McCartney, D. Byrne and M. Turner, "Dietary contributors to hypertension in adults reviewed," *Ir. J. Med. Sci*, vol. 184, p. 81–90, 2015. ([crossref](#))
- [4] R. Eckel, J. Jakicic, J. Ard, J. De Jesus, N. Houston Miller, V. Hubbard, I. Lee, A. Lichtenstein, C. Loria, B. Millen and e. al, "2013 AHA/ACC guideline on lifestyle management to reduce cardiovascular risk: A report of the American college of cardiology/American heart association task force on practice guidelines.," *J. Am. Coll. Cardiol*, vol. 63, pp. 2960-2984, 2014. ([crossref](#))
- [5] L. Schwingshackl and G. Hoffmann, "Mediterranean dietary pattern, inflammation and endothelial function: A systematic review and meta-analysis of intervention trials," *Nutr. Metab. Cardiovasc. Dis*, vol. 24, p. 929–939, 2014. ([crossref](#))
- [6] R. Estruch, E. Ros, J. Salas-Salvado, M. Covas, D. Corella, F. Aros, E. Gomez-Gracia, V. Ruiz-Gutierrez, M. Fiol, J. Lapetra and e. al, "Primary prevention of cardiovascular disease with a Mediterranean diet.," *N. Engl. J. Med.*, vol. 386, p. 1279–1290, 2013. ([crossref](#))
- [7] A. D'Alessandro and G. De Pergola, " The Mediterranean Diet: Its definition and evaluation of a priori dietary indexes in primary cardiovascular prevention.," *Int. J. Food Sci. Nutr.*, vol. 69, p. 647–659., 2018. ([crossref](#))
- [8] W. Willett, F. Sacks, A. Trichopoulou, G. Drescher, A. Ferro-Luzzi, E. Helsing and D. Trichopoulos, "Mediterranean diet pyramid: A cultural model for healthy eating.," *Am. J. Clin. Nutr.*, vol. 61, p. 1402S–1406S, 1995. ([crossref](#))
- [9] C. Davis, J. Bryan, J. Hodgson and K. Murphy, "Definition of the Mediterranean diet: A literature review.," *Nutrients*, vol. 7, p. 9139–9153, 2015. ([crossref](#))

- [10] A. D'Alessandro and G. De Pergola, "Mediterranean diet pyramid: A proposal for Italian people.," *Nutrients*, vol. 6, p. 4302–4316., 2014. ([crossref](#))
- [11] C. R. R. P. F. G. F. a. V. S. D. Stanton, ""Fermented functional foods based on probiotics and their biogenic metabolites.,"" *Current Opinion in Biotechnology*, vol. 16, p. 198–203, 2005. ([crossref](#))
- [12] S. C. Lee and M. H. Foo, "Functional Foods and Its Biomarkers.," in *Introduction to Functional Food Science*, 2nd ed. ed., Richardson, TX: Functional Food Center, 2014.
- [13] M. M. Danik and S. Jaishree, "A new Definition for Functional food by FFC: what makes a new definition unique?," *FFC*, vol. 6, no. 5, pp. 209-223,, 2015.
- [14] S. Lewington, R. Clarke, N. Qizilbash, R. Peto and R. Collins, "Age specific relevance of usual blood pressure to vascular mortality: a meta-analysis of individual data for one million adults in 61 prospective studies.," *Lancet*, vol. 360, p. 1903–1913, 2002. ([crossref](#))
- [15] T. E. Shelly, D. O. Melnnis, E. Pahio and J. Edu, "Aromatherapy in the Mediterranean fruit fly (Diptera Tephritidae): Sterile males exposed to ginger root oil in pre-release storage boxes display increased mating competitiveness in freed-cage trials.," *Journal of Economic Entomology*, vol. 97, no. 3, pp. 846-853, 2004. ([crossref](#))
- [16] M. Taati, M. Alirezaei, M. Meshkatsadat, B. Rasoulilian, A. Kheradmand and S. Neamati, ""Antioxidant effects of aqueous fruit extract of *Ziziphus jujuba* on ethanolinduced oxidative stress in the rat testes.,"" *Iranian J Vet Res*, vol. 39, no. 1, p. 4, 2011.
- [17] Wilson and Ross, "Anatomy and Physiology in Health and Illness", 10th ed ed., Churchill Livingstone, 2006, pp. 80-92.
- [18] K. D. Tripathi, "Essentials of medical pharmacology", 6th ed., Jaypee Brothers Medical, 2013, pp. 135,.
- [19] R. Satoskar, "Pharmacology and Pharmacotherapeutics", 20th ed., Popular Pakistan Pvt Limited, 2011, pp. 402-431.
- [20] R. a. P. T. P. Dr. Gaud, "Modern Patient Counseling", Nirali Prakashan, 2008.
- [21] K. C. Sujit, "Concise Medical Physiology", 6th ed ed., India, New central Book Agency, 2008, pp. 177-180.
- [22] K. B. Devin, ""Idiopathic Intracranial Hypertension", " *Nurosurgery*, vol. 54, no. 3, pp. 538-552, 2004.

- [23] T. Martin, "Hypertension clinical features and investigation," *Hospital Pharmacist*, vol. 14, 2007.
- [24] P. Prakash and N. Gupta, "Therapeutic uses of *Ocimum sanctum* Linn (Tulsi) with a note on eugenol and its pharmacological actions: a short review," *Indian J. Physiol. Pharmacol.*, vol. 49, pp. 125-131, 2005.
- [25] G. P. Kamatou, I. Vermaak and A. M. Viljoen, "Eugenol from the remote Maluku Islands to the international market place: a review of a remarkable and versatile molecule.," *Molecules*, vol. 17, pp. 6953- 6981, 2012. ([crossref](#))
- [26] M. K. Yadav, S. W. Chae, G. J. Im, J. W. Chung and J. J. Song, "Eugenol: a phyto-compound effective against methicillin-resistant and methicillin-sensitive *Staphylococcus aureus* clinical strain biofilms.," *PLoS One*, vol. 10, no. 3, 2015. ([crossref](#))
- [27] W. Van and E. Ben, "Food Plants of the World.," *Timber Press, Inc*, p. 256, 2005.
- [28] L. C. Chiang, "Antiviral activities of extracts and selected pure constituents of *Ocimum basilicum*." *Clin Exp Pharmacol Physiol*, vol. 32, no. 10, pp. 811-6, 2005. ([crossref](#))
- [29] S. Min, A. Fatah, M. Mchael, A. J. M. and Q. S. Xiao, "Effects of fermentation conditions on the potential anti-hypertensive peptides released from yogurt fermented by *Lactobacillus helveticus* and Flavourzyme", vol. 52, pp. 137-145, 2016. ([crossref](#))
- [30] N. C. Cook and S. Samman, "Flavonoids-chemistry, metabolism, cardioprotective effects and dietary source.," *Nutri. Biochem.*, vol. 7, pp. 66-76, 1996.
- [31] J. T. Kumpulainen and J. T. Salonen, "Natural antioxidants and anticarcinogens in nutrition, health and disease.," *Royl. Soci. Chem. UK*, vol. 240, pp. 178-187, 1999. ([crossref](#))
- [32] Pavia, Lampman, Lriz and Vyvyan., "Introduction to Spectroscopy", 5th ed., Cengage Learning, 2015, pp. 577-583.
- [33] A. R. Warsi, "Phytochemical screening and antioxidant activity of ethanolic extract and ethyl acetate fraction from basil leaf (*Ocimum basilicum* L.) By DPPH radical scavenging method.," *Material Science and Engineering*, p. 259, 2017. ([crossref](#))
- [34] J. O. T. Voogt, "Thermal remote sensing of urban climates.," *Remote Sens. Environ.*, vol. 86, p. 370-384., 2003. ([crossref](#))



Copyright © by authors and 50Sea. This work is licensed under Creative Commons Attribution 4.0 International License.



Additions of Tropospheric Ozone (O₃) in Regional Climates (A case study: Saudi Arabia)

Syed Shehzad Hassan¹, Maham Mukhtar³, Ehsan ul Haq², Muneeb Aamir², Hafiz M Rafique¹, Ali Kamran¹, Ghulam Shah², Safer Ali² and Syed Amer Mahmood².

¹ Department of Physics, University of the Punjab Lahore.

² Remote Sensing group Department of Space Science University of the Punjab Lahore Punjab Pakistan.

³ Institute of Management Science (Pak AIMS) Lahore.

*Correspondence | Syed Shehzad Hassan, sshm.mesp72@gmail.com Department of Physics, University of the Punjab Lahore Pakistan.

Citation | Hassan.S.S, Mukhtar.M, Haq.U.E, Aamir.A, Rafique.M.H, Kamran.A, Shah.G, Ali.S and Mahmood.S.A "Additions of Tropospheric Ozone (O₃) in Regional Climates (A case study: Saudi Arabia)". International Journal of Innovations in Science and Technology, Vol 01 Issue 01: pp 33-46, 2019.

DOI | <https://doi.org/10.33411/IJIST/2019010103>

Received | Dec 15, 2018; Revised | Jan 27, 2019 Accepted | Jan 28, 2019; Published | Jan 30, 2019.

ABSTRACT

Anthropogenic activities are responsible for enhancing the concentration of various toxic gases that produces bad Ozone in the troposphere which is harmful to human health. The specific objective of this research was to analyze the spatiotemporal variations in a vertical column of Ozone (O₃) over Saudi Arabia during 2006-2016 using Atmospheric Infrared Sounder (AIRS) onboard AQUA platform and AEROSOL ROBOTIC NETWORK (AERONET) data. The results show that the optical depth of Ozone column varied from 252 Dobson Units (DU) to 264 DU. The main reason of this variation corresponds to the increase in O₃ precursors including Carbon Dioxide (CO₂), Nitrogen Dioxide (NO₂) and Sulfur Dioxide (SO₂). The concentration of CO₂ varied between (379-401) Parts Per Million (PPM), SO₂ varied (3.5x10⁻⁶ - 4x10⁻⁶kg m⁻²) kg m⁻² and NO₂ varies (2.25x10¹⁵ - 2.5x10¹⁵)1/cm² during the investigated timeframe. The results confirm that NO₂ and SO₂ have contributed directly in O₃ formation while CO₂ just increased regional temperatures that enhanced the optical depth of O₃.

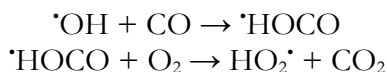
Keywords: AIRS, AERONET, Carbon dioxide, Nitrogen dioxide, Sulfur dioxide, Aerosol optical depth and Dopson Unit.

1. Introduction:

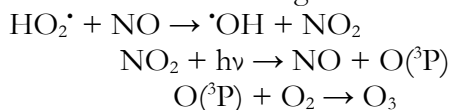
Ozone is the allotropic form of Oxygen [1] which contributes only 0.6 PPM

to the atmospheric composition [2]. Over the last few decades, anthropogenic activities have changed the chemical composition of our atmosphere that influenced the earth's

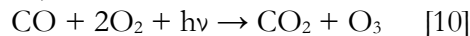
climate by increasing the Ozone level in the troposphere. Two fundamental activities responsible for an increment of Ozone concentration in the atmosphere includes the oxidation of Volatile Organic Compounds (VOCs) and the addition of Non-Methane Hydrocarbons (NMHCs) [3] that resulted in the transportation of Ozone from stratosphere toward troposphere. VOCs are controlled and catalyzed by oxides of nitrogen, carbon and sulfurs. Nitrogen oxides (NO_x), Carbon oxides (CO_x) and Sulfur oxides (SO_x) are formed by the direct combustion of hydrocarbons, volcanic eruptions and biomass burning [4]. Nitrogen oxides affect the tropospheric O₃ because of photochemical reactions [5]. Coal burning in industries and electrical power generators contribute mainly to the production of nitrogen oxides. Therefore, the regions having coal burning plants may be a cause of the increase in Ozone level [6, 1, 2]. Spatiotemporal variations in Ozone vertical column have been analyzed by many researchers [4, 7], they pointed out various sources including hydrocarbon engines, aircrafts and volcanic eruptions responsible for an increment of O₃ in atmosphere. The chemical compounds involved in Ozone formation include carbon monoxide, VOCs and water vapors [8]. The possible reaction of Ozone formation is given below:



Per-Oxy radicals react with nitrogen oxide (NO) to give NO₂, which gives atomic oxygen and nitrogen mono oxide through the phenomenon of photolysis [9]. Radicals of oxygen formed by this process finally convert into Ozone as given below:



The balance of this chemical reactions is as below,



The above discussion verifies that tropospheric ozone is formed by photochemistry of toxic pollutants in the atmosphere. Summer season is proved favorable by many researchers [11, 10, 9] due to high temperatures. The elevated temperature act as catalyst in all chemical reactions like oxidation or reduction of VOCs, hydrocarbons, and the oxides of nitrogen, carbon and Sulphur which are commonly known as Ozone precursors. These oxides play a vital role in bad ozone formation through complex chemical reactions. Therefore, it is significant to investigate the participation of ozone precursors in formation of O₃. The optimum range of these precursors is important to determine for making our environment healthy, clean and green.

The specific objectives of this research were to delineate the spatiotemporal variations in O₃ concentration from 2006 to 2016 over Saudi Arabia. It also aims at describing the contribution of ozone precursors in O₃ formation by direct or indirect chemical reactions. This research will open new avenues for scientists and researchers to control various toxic gasses for a sustainable regional environment.

2. Material and Methods.

Study area.

Saudi Arabia (23.8859⁰ N, 45.0792⁰ E) is situated in the middle east. It is bordered by Yemen, Iraq, Jordan, Oman, Qatar and UAE. Saudi Arabia is a peninsula that is generally described as the region of the desert which receives less rainfall and remain hot throughout the year, while some areas near to the sea are relatively cold [12]. Rain is most likely to fall in February to April in Riyadh, and December to March in eastern Saudi Arabia. In the mountainous zone,

average rain fall is recorded more than 15 inches (50 centimeters) annually. It has an arid and hot climate with harsh weather conditions that sometimes shoot up to 52^o C

at noon in summer season while descends by 0^o C in the night. The spatial extent of the study site is mapped in Figure 1

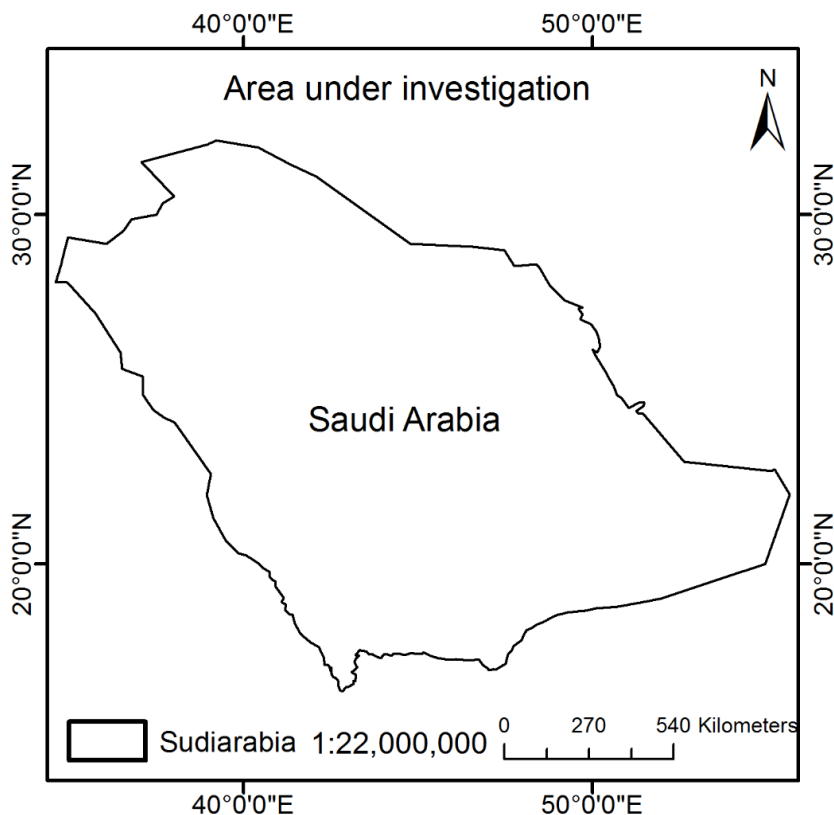


Figure 1. Study site.

Most of industrial expansion occurred during 2000-2016 in Saudi Arabia to boost its economy. The increasing GDP reveals the activism of oil refineries, electrical power plants and coal burning chambers which participated directly or indirectly in O₃ production [13]. We obtained the AErosol RObotic NETwork (AERONET) and Atmospheric InfraRed Sounder (AIRS) data from GIOVAANI to map the temporal changes in O₃.

Methods.

AERONET data.

The AERONET is a constellation of instruments administered by NASA

(Hoben et al., 1998) to establish a balance between atmospheric gasses. AERONET provides valuable information regarding aerosol concentration, their physical properties along with their movement. The AERONET data is available at basic three processing levels: level 1 is under screened: level 1.5 is cloud screened and level 2 is quality assured. The spectral ranges defined for measuring the sky and sun radiances are 340-1020 nm and 440-1020 nm respectively [14]. Aerosol optical depth can be computed by direct sun radiance however, refractive index, scattering albedo and asymmetry parameters can be computed by sky radiance.

We used AERONET data to evaluate the variations in ozone concentration and its optical depth in Dopson Unit (DU) as mentioned below in Table 1

Table 1. Ozone concentration in DU from 2006-2016.

Year	Minimum	Maximum	Average
2006	2.489	3.001	2.745
2007	2.459	3.007	2.733
2008	2.434	2.945	2.69
2009	2.434	3.022	2.728
2010	2.441	2.971	2.706
2011	2.494	3.01	2.752
2012	2.409	2.999	2.704
2013	2.47	2.97	2.72
2014	2.535	3.017	2.776
2015	2.535	3.08	2.81
2016	2.513	2.999	2.756

AIRS data.

The AIRS is an instrument mounted on NASA'S aqua satellite launched on May 04, 2002. AIRS is designed to monitor the variations in concentration of atmospheric gases, air and surface temperature, cloud properties and water vapors. All these observations are taken through infrared technology. It also provides the interpolated spatial patterns for all the gases existing in our atmosphere.

We downloaded time series datasets as recorded by AIRS instrument from GIOVANNI website to study spatiotemporal variations in Ozone concentration with a spatial resolution of 1⁰ (~110km) over the investigation site (Figure 1). The data was acquired only for day timings because the industries produce maximum toxic gases in sunshine hours. Another advantage of data collection for the same hours, was the sharp variations in day-night temperatures due to sandy texture.

High temperature leads to big concentration of Ozone in troposphere [9]. Spatial interpolation techniques [15] are commonly used to plot temporal trends of Ozone fluctuations [16]. The time series graphs of Ozone precursors are compared with graphical variations of toxic gasses to determine similarities and dissimilarities obtained in both graphical and interpolated results that give true representation of our environment [12]. These precursors emit oxides of the Carbon (CO_x), Nitrogen (NO_x) and Sulfur (SO_x) [17] along with VOCs [18]. The oxidation of precursors in presence of sunlight causes formation, transportation [19] and dilution of Ozone in the atmosphere [12]. The main sources of Ozone precursors are petrol pumps, industries, the residual smoke from factories, automobile emissions, water desalination plants and gas-based power stations. The spatial distribution of these plants is listed in the Table 2 as below.

Table 2. Spatial locations of Ozone production plants.

Name	Longitude	Latitude
Al Wafrah kawait	N 28.61751°	E 47.90204°
Wafra Oil Field	N 28.61751°	E 47.90204°
Saudi Aramco Shell Refinery	N 27.0487°	E 49.60696°
Saudi Aramco Total Refining and Petrochemical	N 26.96549°	E 49.50096°
Al Jomaih and Shell Lubricating Oil Company Limited	N 24.54444°	E 46.90587°
Energy Exhibit	N 26.33442°	E 50.12264°
College Preparatory Center - Saudi Aramco	N 26.32536°	E 50.13654°
Hawtah GOSP	N 22.98034°	E 46.90237°
Haradh Airport - Saudi Aramco	N 24.09982°	E 49.22364°
Shaybah Airport - Saudi Aramco	N 22.51454°	E 53.96415°
Luberef	N 21.4438°	E 39.18362°
SAMREF	N 23.98153°	E 38.2406°
Schlumberger Dowell	N 25.18383°	E 49.3888°
Awad Al-Joufi Trading Est.	N 26.94077°	E 49.67782°
Vetco Saudi Arabia (Brandt Fluid Control)	N 26.24536°	E 50.19992°
Tanajib Aramco Plant	N 27.81885°	E 48.86989°
Schlumberger UDH Shared Base	N 25.18754°	E 49.38922°
Saudi Aramco Pump Station No. 3	N 25.16647°	E 47.50244°
Ain Dar GOSP #2	N 25.97216°	E 49.23185°
Prosperity Well	N 26.32112°	E 50.12779°
Saudi Aramco Total Refining And Petrochemical	N 26.96549°	E 49.50096°
Saudi Aramco Pump Station 5	N 24.79937°	E 45.84033°
Saudi Aramco Pump Station 7	N 24.59831°	E 44.14159°
Saudi Aramco Pump Station 8	N 24.47973°	E 43.37974°
Saudi Aramco Pump Station No. 6	N 24.70129°	E 44.97734°
Hawtah GOSP	N 22.98034°	E 46.90237°
LUBEREF (Saudi Aramco Base Oil Company	N 23.94335°	E 38.31482°
Luberef	N 21.4438°	E 39.18362°
Saudi Aramco - Yanbu Refinery	N 23.94883°	E 38.29813°
شركة ياسرف - شركة ينبع أرامكو سينوبك للتكرير	N 23.96394°	E 38.28508°
Saudi Aramco Shell Refinery	N 27.0487°	E 49.60696°
Saudi Aramco - Jeddah Refinery	N 21.45123°	E 39.18111°
Jizan Bulk Plant - Saudi Aramco	N 16.87137°	E 42.56498°
Schlumberger Dowell	N 25.18383°	E 49.3888°

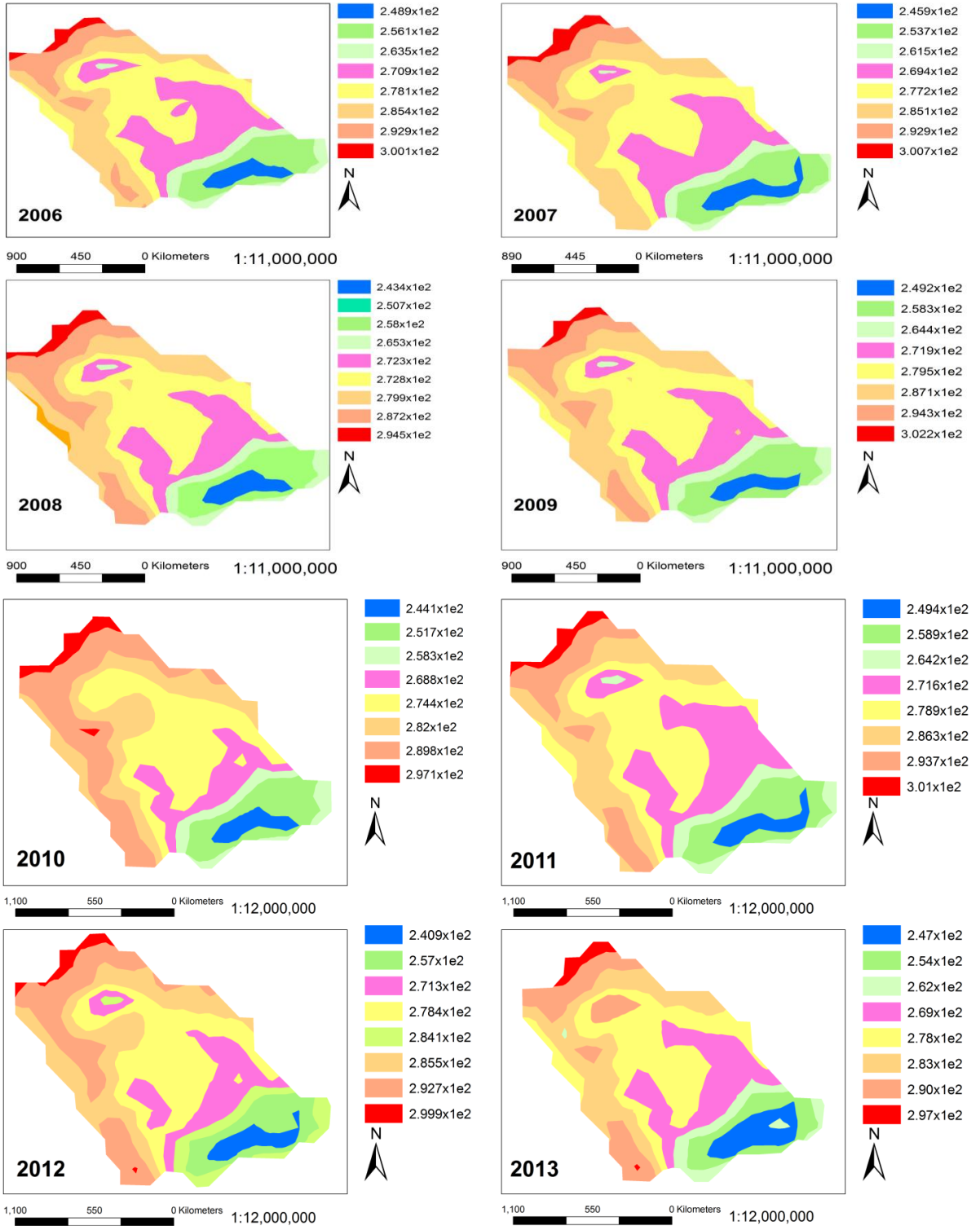
ارامكو السعودية مصفاة الرياض	N 24.52621°	E 46.88242°
Tanajib Aramco Plant	N 27.81885°	E 48.86989°
Ain Dar GOSP #2	N 25.97216°	E 49.23185°
Samsung Engineering - CBDC Project Site Office	N 24.1377°	E 52.69218°
Al Jubail	N 26.96549°	E 49.50096°

Regression is a set of statistical processes for estimating the relationship among variables [20]. We used the linear regression to determine the contribution of each pollutant in formation of bad Ozone over Saudi Arabia for the investigated period.

1. Results.

Spatiotemporal variations in Ozone vertical column are mapped in Figure 2 which shows that North west of Saudi Arabia is completely occupied by bad ozone in comparison to south east. The concentration of the Ozone was observed maximum at spatial location (33° N and 40° E) in all the

maps of Figure 2 and minimum at (20° N and 50° E). The highest value of bad ozone was recorded as 300DU in comparison to the lowest as 244 DU. Red zones in Figure 2 were found with large number of anthropogenic activities. About 79% of industries, power plants and oil refineries mentioned in Table 2 were actually existing in the North west of Saudi Arabia that mainly contributed in formation of bad ozone. While, the blue areas in Figure 2 were found comparatively less polluted. The trend shows that the spatial extent of red and orange zones is increasing speedily toward south which is very alarming situation.



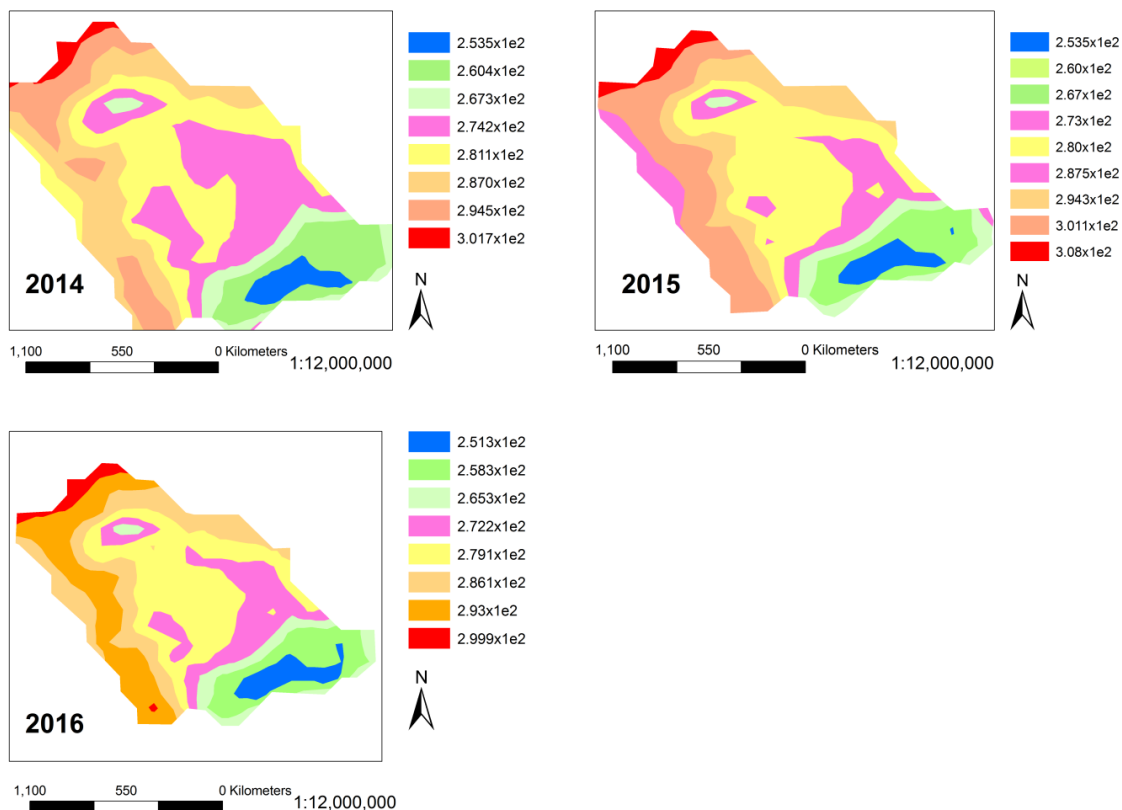


Figure 2: Spatiotemporal variations in Ozone vertical column with spatial resolution of 1 deg from 2006 –2016 over Saudi Arabia

5.1 Concentration of toxic gasses in comparison to GDP of Saudi Arabia.

AERONET data provided us annual variations in the concentration of toxic gasses (CO₂, SO₂ and NO₂) emitted by combustion chambers of industries existing in Saudi Arabia as mentioned in Table 3.

These pollutants were found responsible for O₃ formation by chemical reaction. Industrial activism is a term used for the regions where GDP is increased rapidly. We collected the annual increment in GDP of Saudi Arabia from World Bank as mentioned in Table 3

Table 3. Annual variations in concentration of toxic gasses against GDP and O₃.

Year	Ozone DU	SO ₂ Kgm ⁻² (1x10 ⁸)	NO ₂ 1/cm ⁻² (1x10 ¹²)	CO ₂ PPM	GDP B USD	Ozone DU
2006	295	353	225	378	376	2.745
2007	296	344	220	382	416	2.733
2008	297	355	225	384	519	2.69
2009	298	410	226	377	429	2.728
2010	304	415	229	368	528	2.706
2011	305	420	230	364	671	2.752
2012	305	425	240	391	736	2.704

2013	306	430	270	395	746	2.72
2014	307	460	280	397	756	2.776
2015	309	480	295	400	654	2.81
2016	314	500	300	402	646	2.756

These variations are plotted as below in Figure 3.

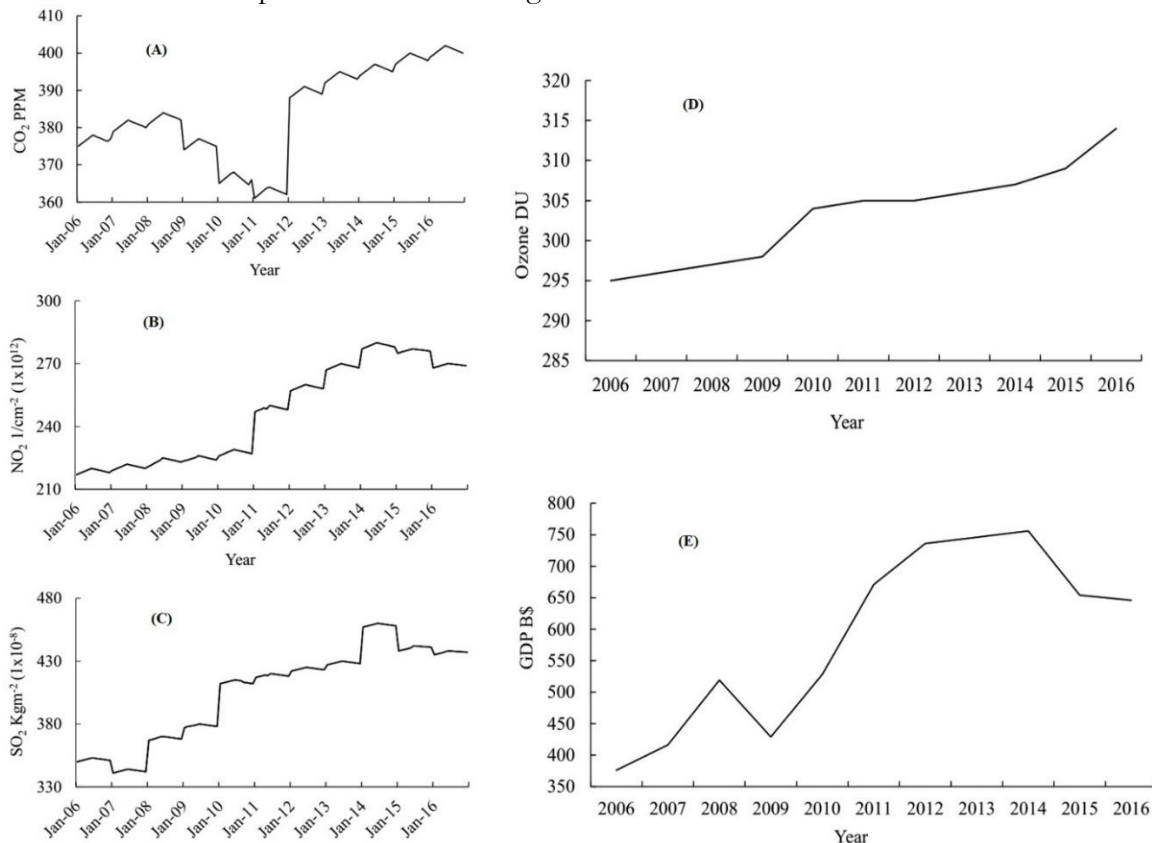


Figure 3. Variations in CO₂, SO₂, NO₂, O₃ and GDP during 2006-2016.

Figure 3(A) is showing an increasing trend for CO₂ concentration that varied from 378 PPM in 2006 to 402 PPM in 2016. This increased level of CO₂ created a natural greenhouse effect resulting in increment to regional temperatures. Figure 3(B) determines that the highest value of NO₂ was

recorded in the year 2014 in comparison to 2006. The concentration of Nitrogen oxide was recorded as 2.25×10^{15} 1/cm² in 2006 that increased to 3×10^{15} 1/cm² in 2016. Sunlight dissociates nitrogen dioxide into nitric oxide and oxygen atoms as follows



A single atom of oxygen combines with the oxygen molecule to give Ozone as below,



Similarly, SO₂ is showing the same trend in Figure 3(C) as NO₂ in Figure 3(B). SO₂ reacts with ultraviolet light and produces an Ozone precursor (O). Variations in SO₂

were observed in mole fraction that varied from 3.5×10^{-6} kg m⁻² in 2006 to 4×10^{-6} kg m⁻² in 2016. Possible reactions of Sulphur that

contributes in Ozone formation are given below,

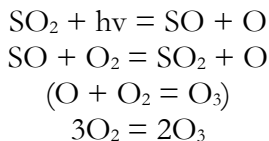


Figure 3(D) is showing that the concentration of O₃ is continuously increasing in the troposphere due to oxidation of ozone precursors. We applied a linear regression model to determine the

relationship between Ozone and the GDP. We found a strong relationship between these two variables with R²=0.858 as shown in Figure 4

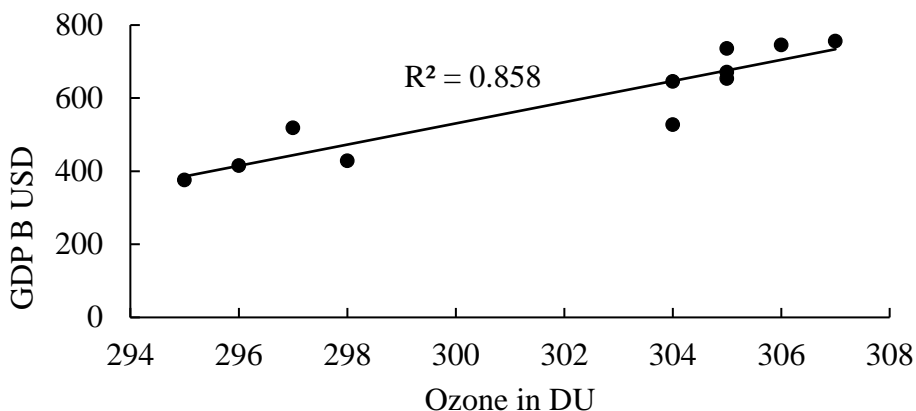


Figure 4. Linear regression applied to GDP (Billion USD) against Ozone concentration in DU.

The regression analysis applied in Figure 4 verifies that the industrial revolution in Saudi Arabia has not only increased the GDP but also a penalty of ozone precursors is being added in the troposphere by industries/oil refineries that produced harmful O₃ in access through oxidation/reduction processes. Such ozone is harmful not only for humans but the whole ecological balance is disturbed badly.

We assumed three types of ozone precursors to evaluate the contribution of each precursor in O₃ formation. To do so, a linear regression is applied to the concentration of NO₂, SO₂, CO₂ against the GDP. As we have proved in Figure 4 that GDP and O₃ are in direct relation with each other. The results of linear regression are mention in Figure 5 as below.

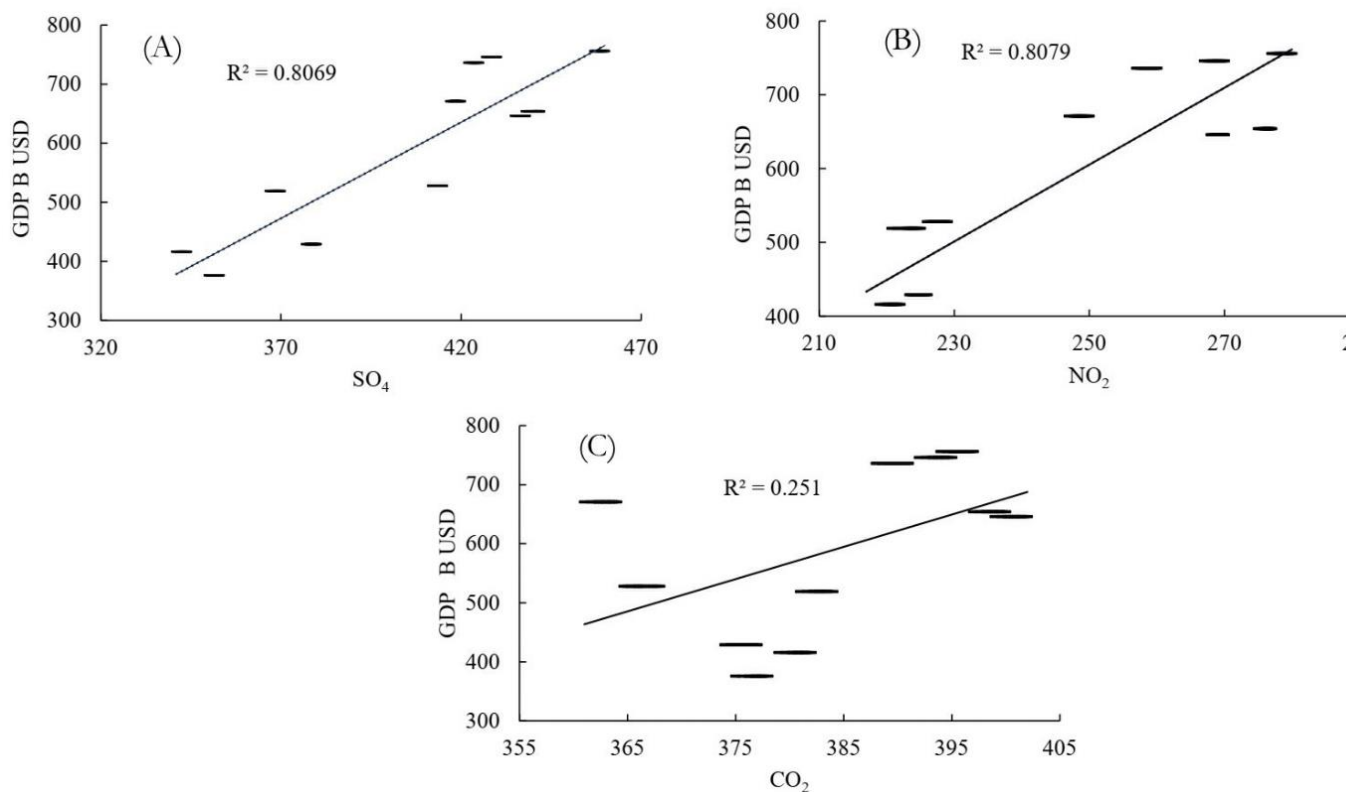


Figure 5. Linear regression applied to Ozone precursors (NO₂, SO₄ and CO₂) against GDP.

Figure 5 (A,B) are showing fair relationship with coefficients of determination as 0.8069 and 0.8079 respectively which is a clear proof that SO₄ and NO₂ contributed directly in O₃ formation. On the other hand, there exist a very weak relation between CO₂ and GDP with R²=0.251 which indicates that CO₂ did not contribute directly in O₃ formation but it raised the regional temperatures and this elevated temperature catalyzed the oxidation of ozone precursors.

5. Discussion

Nitrogen dioxide and sulfur dioxide are the precursors of the Ozone, which decompose into their components in day timing in the presence of light and form Ozone by oxidation/reduction. These precursors were identified by environmental protection department of Saudi Arabia in collaboration

with NASA. They found that the concentration of nitrogen dioxide and Sulphur dioxide is increased by 0.05% annually. These gases produced natural greenhouse effect by capturing thermal radiations that played a vital role in Ozone formation by making conducive environment for photolysis. Oil refineries, petrol pumps and water purification plants are the main sources of production of nitrogen dioxide and sulfur dioxide. Sunlight act as catalyst in oxidation of Nitrogen and Sulphur which are detergents for ozone formation. Nitrogen is highly electronegative element with a lone pair after completion of its octet. This lone pair creates an effect of electrostatic interaction between partial positive and partial negative elements. Partial positive charge creates due to electro negativity difference between the bonding

molecules. Therefore, the coulomb's interaction between partial positive and partial negative element weaken the nitrogen bond with oxygen. When sunlight hit this weak bond, the nitrogen dioxide dissociates into nitrogen mono oxide and oxygen radical. Oxygen radical interacts with the already existing oxygen molecule and produces Ozone.

The spatiotemporal variations in Ozone vertical column were observed due to enhanced nitrogen dioxide and sulfur dioxide in the atmosphere. It was observed that CO₂ was not directly involved in Ozone formation. The spatial locations with elevated Ozone concentration were observed

having elevated temperatures, which reveals that high temperature expedites the process of oxidation and reduction. The increase in Ozone concentration was recorded by 1.2% per year from 2006 to 2016.

7. Conclusion

There exists a global race to build regional economies through industrialization. This industrial revolution is responsible for addition of various toxic gasses in our environments which are dangerous for human survival and sustainable development. Therefore, efficient ways are required to handle these pollutants to save our environments for a green future.

8. Acknowledgement

We would like to acknowledge the profound services of NASA for providing reliable global data at Giovanni website (<http://giovanni.gsfc.nasa.gov/>).

8. References:

References

- [1] Ryan D. McCulla, "Atomic Oxygen O(3P): Photogeneration and Reactions with Biomolecules.," ACS Chemistry for life, 2010.
- [2] A. G. Streng, ""Tables of Ozone Properties".," *Journal of Chemical Engineering Data.*, vol. 6, no. 3, p. 431–436., 1961. ([Crossref](#))
- [3] G. a. Tzanis, "Study of stratosphere-troposphere exchange events of Ozone in India and Greece using Ozonesonde ascent.," *Meteorological applications*, vol. 18, no. 4, pp. 467-474, 2011.
- [4] Fishman et al., "Ozone in the boundary layer of the equatorial Atlantic Ocean," *Tellus B*, vol. 3, pp. 314-322, 1989.
- [5] Vukovich, "A time dependant photochemical model of Ozone near the ground.," *geophysical research*, vol. 81, 1976.
- [6] G. A., R. Shukla, S. Bhattacharya and V. Dadhwal, "Subregion (district) and sector level SO₂ and NO_x emissions for India: assessment of inventories and mitigation flexibility," *Atmospheric Environment*, vol. 35, pp. 703-713, 2001. ([Crossref](#))

- [7] L. Chan, L. H.Y., K. Lam and T. Wang, "Analysis of seasonal behavior of tropospheric Ozone at Hong Kong.," *Atmospheric Environment*, vol. 32, pp. 159-168, 1998. ([Crossref](#))
- [8] J. Stedman and M. Williams, "A trajectory model of the relationship between Ozone and precursor emissions.," *Atmospheric Environment*, Vols. 26A,, pp. 1271-1281, 1992. ([Crossref](#))
- [9] J. Allen, "Tango in the Atmosphere: Ozone and Climate Change," *NASA Earth Observatory*, 2004.
- [10] J. R. Barker, Problems and Progress in Atmospheric Chemistry, vol. 3, Advanced Series in Physical Chemistry, Ed., Singapore: World Scientific, 1995.
- [11] J. M. Prospero, P. Ginoux, O. Torres, S. E. Nicholson and T. E. E. Gill, "Environmental characterization global sources of atmospheric soil dust identified with the Nimbus 7 total ozone mapping spectrometer (TOMS) absorbing aerosol product.," *Rev. Geophys*, vol. 40, p. 1002, 2002. ([Crossref](#))
- [12] J. H. Seinfeld and S. N. Pandis, Atmospheric Chemistry and Physics - From Air Pollution to Climate Change., Vols. ISBN 0-471-17816-0, John Wiley and Sons, 1998.
- [13] C. R., G. R. and G. A., "Ultraviolet radiation and ground-level Ozone variation in Lithuania.," *Journal of Environmental Engineering and Landscape Management*, vol. 1, pp. 31-36, 2004.
- [14] B. N. Holben, T. F. Eck, I. Slutsker, D. Tanré, J. P. Buis, A. Setzer, E. Vermote, J. A. Reagan, Y. J. Kaufman, T. Nakajima, F. Lavenu, I. Jankowiak and A. Smirnov, "AERONET-A federated instrument network and data archive for aerosol characterization," *Remote Sensing of Environment*, vol. 66, pp. 1-16, 1998. ([Crossref](#))
- [15] Liji Mary David, I. A. Girach and P. R. Nair, "Distribution of Ozone and its precursors over Bay of Bengal during winter," *Role of meteorology*, vol. 29, 2009. ([Crossref](#))
- [16] Eric Grosjean and D. Grosjean, "Formation of Ozone in Urban Air by Photochemical Oxidation of Hydrocarbons: Captive Air Experiments in Porto Alegre," *RS Journal of the Brazilian Chemical Society*, vol. 9, 1997. ([Crossref](#))
- [17] Hesham A. Al-Jeelani et al., "Diurnal and Seasonal Variations of Surface Ozone and Its Precursors in the Atmosphere of Yanbu, Saudi Arabia," *Journal of Environmental Protection*, vol. 5, pp. 408-422, 2014. ([Crossref](#))

- [18] Amann, Derwent and Forsberg, Health risks of Ozone from long-range transboundary air pollution, ISBN 978-92-890-4289-5 ed., Publication of World Health Organization Europe, 2008.
- [19] Huff and K. ., "The Effects of Volcanic Sulfur Dioxide on the Ozone Layer," *Atmospheric Chemistry*, 1996.
- [20] Liuja, Bailang Yu, Zuoqi Chen, Baiiang Li and J. Wu., "Investigating the Temporal and Spatial Variability of Total Ozone Column in the Yangtze River Delta Using Satellite Data: 1978–2013," *Remote Sens.*, vol. 6, pp. 12527-12543, 2014. ([Crossref](#))



Copyright © by authors and 50Sea. This work is licensed under Creative Commons Attribution 4.0 International License.